Development and Validation of Speed Loss for a Blunt-shaped Ship in Two Rough Sea Voyages in the Southern Hemisphere

Sasa, Kenji ; Faltinsen, Odd M. ; Lu Li-Feng ; Sasaki, Wataru ; Jasna, Prpić-Oršić ; Jasna, Kashiwagi ; Kashiwag, Masashi ; Ikebuchi, Takuro

(Citation)
Ocean Engineering,142(15):577-596

(Issue Date)
2017-09

(Resource Type)
journal article

(Version)
Accepted Manuscript

(URL)
https://hdl.handle.net/20.500.14094/90005321

Development and validation of speed loss for a blunt-shaped ship in two rough sea voyages in the Southern Hemisphere

Kenji Sasa[1,*]

5-1-1, Fukae Minami Machi, Higashinada-ku, Kobe, 658-0022 JAPAN

Odd Magnus Faltinsen[2], Li-Feng Lu[1], Wataru Sasaki[3], Jasna Prpić-Oršić[4], Masashi Kashiwagi[5], Takuro Ikebuchi[6]

Abstract

Maritime transportation is becoming increasingly complex owing to the fluctuation of oil prices, the introduction of environmental guidelines, and the onset of climate change. Although optimal routing has been researched for decades, few studies have investigated speed loss in rough waves for ships with blunt shape and low speed. Onboard measurement of a 28,000DWT bulk carrier has been conducted for six years in rough sea voyages in the Southern Hemisphere. It is necessary to validate the wave and wind conditions in order to discuss speed loss in these situations. Here, numerical simulation of speed loss is developed and conducted for each estimated wave condition. The speed losses under different numerical models of added resistance are quantitatively compared in two rough sea voyages. The simulated results of speed loss are in good agreement with the measured results if the

*Corresponding Author
Email address: sasa@maritime.kobe-u.ac.jp (Kenji Sasa)
[1]Dept. of Maritime Sciences, Kobe University
[2]Centre for Autonomous Marine Operations and Systems, Norwegian University of Science and Technology
[3]Wind Energy Institute of Tokyo, Inc. (Japan Agency for Marine-Earth Science and Technology)
[4]Faculty of Engineering, University of Rijeka
[5]Dept. of Naval Architecture and Ocean Engineering, Osaka University
[6]Imabari Shipbuilding Co., Ltd.

estimated wave is accurate and the wave direction is properly defined. The speed loss accuracy is significantly influenced by the wave estimation accuracy or wave direction setting compared to that in the numerical models of added resistance in actual seas. Simulated results provide important information to evaluate the performance of a ship with blunt shape in rough waves.

Keywords: Speed loss, added resistance, wave estimation, engine control, fuel oil consumption, gas emission, numerical simulation

1. Introduction

Optimal ship operation is one of the most important objectives in the maritime industry. Numerous studies have investigated various evaluation methods for optimal ship routing in previous decades (Hanssen, et al., 1960) (Maki, et al., 2011) (Komas, et al., 2012) (Lin, et al., 2013). Some objective functions for optimal routing, such as safety, voyage time, and fuel oil consumption, vary with the demand or circumstances in a particular era. Since the Energy Efficiency Design Index (EEDI) was introduced in 2012, gas emission has emerged as a major concern (Prpić-Oršić, et al., 2012). Various studies have investigated the optimization of the ship shape, main engine, and propellers (Devanney, 2011) (Butterworth, et al., 2015). To minimize gas emission and fuel oil consumption, the concept of a future ship, namely "Eco ship 2030", has been proposed (NYK, 2009). Optimal ship routing encompasses many fields, such as weather forecasting, seakeeping, propulsion, and machinery. A seafarer's intuition or experience is not sufficient to meet the requirements of optimal ship routing in terms of ship design and operation. Major meteorological organizations, such as the National Centers for Environmental Prediction (NCEP) (Kalnay, et al., 1996) and the European Centre for Medium-Range Weather Forecasts (ECMWF) (Dee, et. al., 2011), provide a downloadable global weather database. This database has been employed in various fields to determine the weather conditions and thus achieve reliable optimal ship routing in the Northern Hemisphere (Vettor, et al., 2016). However, the reliability of optimal routing in the Southern Hemisphere has not been investigated extensively thus far. The authors have already demonstrated the accuracy of wave estimation for three cases of rough sea voyages in the Southern Hemisphere using measured data of a 28,000DWT-class bulk carrier through numerical wind and

wave simulations (Lu, et al., 2017). It has been shown that the simulated winds are not necessarily in agreement with the measured ones. In particular, wind speed differences of 3 $\sim$ 10 m/s and wave height differences of 1 $\sim$ 3 m might exist between the NCEP and the ECMWF data for simulations in the Southern Hemisphere. In previous decades, many studies have investigated the added resistance and relative motion of vessels in the field of seakeeping (Faltinsen, 1993). Three-dimensional methods continue to suffer from problems in practical applications (Yasuda, et al., 2016), while time-domain methods involve a long computation time. Therefore, the strip theory remains the main method for evaluating the ship response and added resistance for optimal routing (Prpić-Oršić, et al., 2012). On the other hand, unified theories have been derived from the strip theory (Newman, 1978). Kashiwagi et al. proposed the Research Initiative on Oceangoing Ships (RIOS), which is a novel system for evaluating ship performance in actual seas (Kashiwagi, et al., 2004). The seakeeping part of this system is based on the enhanced unified theory (EUT) (Kashiwagi, 1992). This method considers the three-dimensional problem in the outer region, and the solution is obtained by matching the outer solution with the inner solution obtained for a two-dimensional problem. The computed results have been shown to be nearly identical to the results of model tests. Speed loss of a ship can be modeled in combination with propulsion and machinery models (Faltinsen, et al., 1980) (Bondarenko, et al., 2011). Although many studies have estimated speed loss in a seaway, few have compared their results with measurements made in actual seas. Moreover, few studies have compared the strip method and EUT in terms of the total speed loss in a seaway. In the present study, these aspects are examined using the measured data of a bulk carrier in rough sea voyages in the Southern Hemisphere on the basis of the relation between the total thrust and the resistance. Remarkable speed losses are measured owing to extremely rough wave conditions (5 $\sim$ 7 m). Further, various parameters are analyzed to evaluate the speed loss in irregular waves with the ventilation of the propeller. Speed losses in two rough sea voyages are simulated considering different wave conditions and seakeeping models. Finally, the overall accuracy is evaluated on the basis of the ship's speed, engine power, CO_2 emission, etc., for vessels with blunt shape and low speed in rough seas of the Southern Hemisphere.

2. Onboard Measurement of Ship Performance

Techniques for monitoring ships in actual seas have been developed in recent decades. Owing to the development of network technologies, onshore monitoring of ships is becoming increasingly common. However, most of the information collected by these techniques is confidential and hence scarcely available. Moreover, there are not many examples of ships with blunt ship shape and low speed. Onboard measurement of the performance of a 28,000DWT class bulk carrier was underway for six years from July 2010 to August 2016 (Lu, et al., 2017). The ship is a tramper without regular routes. The management company changed in 2012, and there have been some changes in the navigation routes, engine operations, etc., since then. In particular, the main routes have been defined between Asian countries and locations in the Southern Hemisphere, such as Oceania or South America, after the change in ship management. The sea conditions in the Southern Hemisphere are believed to be rougher than those in the Northern Hemisphere, because the former has fewer landmasses. The authors have shown that remarkable difficulties were encountered during voyages in the Tasman Sea and the Atlantic Ocean as well as off the coasts of South Africa and Australia in 2013 $\sim$ 2016. The main dimensions of the ship are listed in Table 1. In this study, speed losses are discussed for the measurements made in the Southern Hemisphere. Figures 1 and 2 show the measured parameters, including the ship's motion, speed, engine revolution, engine power, fuel oil consumption, and exhaust gas temperatures on six cylinders of the main engine, on June 1 $\sim$ 4 (Case A) and June 14 $\sim$ 16 (Case B), 2013. Ship motion is expressed as significant values obtained by the zero-up cross method for a 10-min time series every 0.1 s. Other parameters are shown as averaged values for a 10-min time series every 1 s. Some of the tendencies can be summarized as follows.

(1) Very large ship motion, i.e., 15° of roll and 5° of pitch, occurred in rough sea conditions.

(2) Very strong wind speeds were measured in Case A (around 15 $\sim$ 25 m/s) for two days. Relatively strong wind speeds were measured in Case B (around 10 $\sim$ 20 m/s).

(3) Remarkable speed losses occurred in each case. In particular, the ship's speed reached a minimum value of 2 $\sim$ 3 knots in Case A. Thus, the ship nearly lost all its propulsion force against the total resistance in rough seas. The engine revolutions were reduced simultaneously from 109 rpm to 90 $\sim$

100 rpm over 10 min on average.
(4) The engine power, thrust, and fuel oil consumption were nearly constant in Cases A and B despite remarkable reduction in the ship's speed and engine revolution. It was assumed that the ship resistance prevents the ship from moving forward, even if propulsion force is supplied from the main engine. The engine control can be regarded as constant power control (or constant torque control) in Cases A and B.
(5) The exhaust gas temperature is one of the important factors affecting the intentional engine operation in rough sea voyages. The average temperature was 340 $\sim$ 380 C in all the cases. The temperature in one of the cylinders showed the highest values (around 370 $\sim$ 380 C). These values were nearly equal to those under 85% to 100% load condition in the test run. This implies that the main engine could be overloaded in such rough sea voyages. There is a possibility that the revolution (or injection of fuel oil) was manually controlled to not exceed an exhaust gas temperature of 370 C. The speed losses were numerically simulated for Cases A and B, which can be regarded as cases of constant power control of the main engine.

3. Estimation Method of Speed Loss

A ship's speed is determined by the relation between its thrust and resistance. A seaway presents different types of resistance, both in still water and in waves. The former is defined as the resistance in still water, and the latter is defined as the added resistance. The following subsections briefly describe numerical methods for reproducing each force related to speed loss analysis.

3.1. Ship Resistance in Still Water

Various resistance forces act on a ship, and they increase with the ship's forward speed, V. A ship's resistance in still water is expressed as

$$R_{SW}(V) = (1+k_1)R_F(V) + R_W(V) + R_{APP}(V) + R_B(V) + R_{TR}(V) + R_A(V) \tag{1}$$

where R_{SW} is the total resistance in still water, R_F is the resistance due to friction, R_W denotes the wave-making and wave-breaking resistance, R_{APP} is the resistance of the ship's appendages, R_B is the additional pressure resistance of the bulbous bow near the water surface, R_{TR} is the additional pressure resistance of the immersed transom stern, R_A is the model-ship

correlation resistance, and $(1 + k_1)$ is the form factor describing the viscous resistance of the hull in relation to R_F. In this study, the empirical method is used (Holtrop, et al., 1982) (Holtrop, 1984). It is difficult to estimate the form factor by using the potential theory because it includes a strong viscous component. Some formulas have been proposed. Here, we use the formula proposed by MARINTEK, which is expressed as

$$1 + k_1 = 1 + 0.6\gamma + 75\gamma^3 \tag{2}$$

$$\gamma = \frac{C_b}{L_{pp}}\sqrt{(d_F + d_A)B} \tag{3}$$

where C_b is the block coefficient, and d_F and d_A are the forward and aft perpendicular drafts. The viscous component, $R_F(V)$, is modeled as

$$R_F(V) = \frac{1}{2}\rho S V^2 C_F \tag{4}$$

where ρ is the water density, S is the wetted area of the ship, and C_F is the coefficient of frictional resistance, which is calculated by the formula proposed by ITTC (International Towing Tank Committee), where the roughness of the ship hull, ΔC_F, is given by

$$C_F = C_{F,ITTC} + \Delta C_F \tag{5}$$

$$C_{F,ITTC} = \frac{0.075}{\left(\log_{10} R_n - 2\right)^2} \tag{6}$$

$$\Delta C_F = \left\{111\left(AHR \cdot V\right)^{0.21} - 404\right\}\left(\frac{0.075}{\left(\log_{10} R_n - 2\right)^2}\right)^2 \tag{7}$$

where R_n is the Reynold's number shown in Eq. (8), and AHR is the averaged surface roughness of the ship hull ($75 \sim 150\ \mu m$).

$$R_n = V \times \frac{L}{\nu} \tag{8}$$

where, L is the ship's length and ν is the dynamic coefficient of viscosity ($=10^{-6}\mathrm{m}^2/\mathrm{s}$).

3.2. Estimation of Added Resistance

Two types of methods are used to estimate the added resistance. One is the pressure integration method for a ship in waves. Here, the conservation of momentum following Maruo's theory is used (Kashiwagi, 1991). The added resistance is calculated as

$$\begin{aligned}\frac{R_{AW}(\omega,\chi,V)}{\rho g\zeta^2} &= \frac{1}{4\pi k_0}\left[-\int_{-\infty}^{k_1}+\int_{k_2}^{k_3}+\int_{k_4}^{\infty}\right]\left\{|H_C(k)|^2+|H_S(k)|^2\right\} \\ &\times \frac{\kappa(k,V)\left\{k-k_0\cos(\chi-\pi)\right\}}{\sqrt{\kappa^2(k,V)-k^2}}dk \end{aligned} \tag{9}$$

where R_{AW} is the added resistance in waves, ω is the circular frequency, χ is the relative wave direction (0° is defined as ship bow), ρ is the water density, g is the acceleration due to gravity, ζ is the wave amplitude, k_0 is the wave number of the incident wave, and $H_C(k)$ and $H_S(k)$ are the Kochin functions that correspond to the symmetric mode and asymmetric mode, respectively. Further, $\kappa(k)$ is expressed as

$$\kappa(k,V)=\frac{1}{g}\left(\omega+kV\right)^2=K+2k\tau+\frac{k^2}{K_0} \tag{10}$$

$$K=\frac{\omega^2}{g},\ \ \tau=\frac{V\omega}{g},\ \ K_0=\frac{g}{V^2} \tag{11}$$

where τ is the Hanaoka parameter (Hanaoka, 1976). In addition, k_1, k_2, k_3, and k_4 are the wave numbers of the k_1 and k_2 wave systems, expressed as

$$\left.\begin{matrix}k_1\\k_2\end{matrix}\right\}=-\frac{K_0}{2}\left(1+2\tau\pm\sqrt{1+4\tau}\right) \tag{12}$$

$$\left.\begin{matrix}k_3\\k_4\end{matrix}\right\}=-\frac{K_0}{2}\left(1-2\tau\mp\sqrt{1-4\tau}\right) \tag{13}$$

The two Kochin functions are obtained from the EUT and the new strip method (NSM) (Salvessen, et al., 1970) (Fujino, et al., 1982). In the EUT, the Kochin function is obtained from the source strength and the doublet in the outer problem. This is described in detail in (Kashiwagi, 1992). It can be obtained using a similar technique in the NSM. The diffraction component

of the added resistance for a short wave length cannot be ignored for blunt-shaped ships, and two formulas are considered in the high frequency region (Faltinsen, et al., 1980) (Okusu, 1986). They are expressed as

$$\frac{R_{AW}^{A}(\omega,\chi,V)}{\rho g\zeta^{2}} = \frac{1}{2}\int_{L}\left\{\sin^{2}(\theta+\chi)+\frac{2\omega_{0}V}{g}\left(1-\cos\theta\cos(\theta+\chi)\right)\right\}n_{1}d\ell \tag{14}$$

$$\frac{R_{AW}^{A}(\omega,\chi,V)}{\rho g\zeta^{2}} = \frac{1}{2}\left(1+\frac{2\omega_{0}V}{g}\right)\int_{-B/2}^{B/2}\frac{K_{1n}}{k_{0}}n_{1}dy \tag{15}$$

$$K_{1n} = \frac{\left(\omega_{e}-k_{0}V\cos^{2}\theta\right)^{2}}{g}\sin(\varphi-\theta) \tag{16}$$

where R_{AW}^{A} is the added resistance as the diffraction component in the high frequency region, θ is the angle between the longitudinal line and the tangential line at the water line of ship, φ is the angle between the reflected wave and the ship's hull, n_1 is the normal vector in longitudinal direction at the calculation point, and ω_e is the encounter frequency. The added resistance due to wind is expressed as

$$R_{WD}(U_{W},\theta_{W}) = \frac{1}{2}\rho_{a}C_{X}(\theta_{W})A_{X}U_{W}^{2} \tag{17}$$

where ρ_a is the air density, C_X is the coefficient of wind resistance in the longitudinal direction, A_X is the front wind area, θ_W is the wind direction and U_W is the wind speed. Further, C_X is defined by Fujiwara's method (Fujiwara, et al., 1998).

3.3. Estimation of Deducted Thrust

If a ship's motion increases in waves, the relative surface elevations around the ship will vary. Therefore, the propeller must be sufficiently submerged in the water to generate propulsion force. However, the propeller sometimes emerges from the water because of the relative surface elevation. This causes a reduction in the propulsion force, which is called ventilation. Studies on the thrust reduction in waves have been conducted (Faltinsen, et al., 1980). Smogeli expressed it as a function of the propeller speed and the vertical distance between the propeller and the water surface (Smogeli, 2006). Figure 3 shows the thrust reduction function, β_{TV}, for an open propeller. In the

present study, the thrust reduction is modeled as a combination of the linear functions of propeller speed and relative surface elevation as follows:

$$\beta_{TV}(n,h) = f(n/n_{bp}, h/R) \tag{18}$$

where n is the propeller speed, n_{bp} is the bollard pull speed of the propeller, h is the vertical distance between the propeller and the water surface, and R is the radius of the propeller. The relative surface elevation at the position of the propeller, $\zeta_r(x_p)$, is required to obtain the value of h as follows:

$$h = h_p + \zeta_r(x_p) \tag{19}$$

$$\zeta_r(x_p) = \xi_3 + y_P\xi_4 - x_P\xi_5 - \varphi_0 \tag{20}$$

where h_P is the depth of the propeller in still water, $\xi_i (i = 3, 4, 5)$ represents the motion amplitudes for heave, roll, and pitch according to the EUT and the NSM, and φ_0 is the velocity potential of the incident waves. Thus, the thrust reduction factor, β_{TV}, can be obtained by Eq. (18).

3.4. Ship Thrust in Still Water

The propulsion force is also important for evaluating the speed loss, and it is estimated on the basis of the experimental results for the B-series propeller in open water (Oosterveld, et al., 1975). The thrust and torque coefficients are expressed as polynomials, and the thrust and torque of a ship are expressed as

$$T(n,V) = \rho n^2 D^4 K_T \tag{21}$$

$$Q(n,V) = \rho n^2 D^5 K_Q \tag{22}$$

$$Q_B(n,V) = \rho n^2 D^5 \eta_R K_Q \tag{23}$$

where T is the thrust of the propeller, Q is the torque of the propeller in open water, and Q_B is the torque of the propeller considering ship's hull, n is the propeller speed, D is the diameter of the propeller, η_R is the propeller efficiency (= 0.98), K_T is the thrust coefficient, and K_Q is the torque coefficient. Coefficients, K_T and K_Q, should be defined from the experiment data for the ship. However, the detail of thrust and torque properties cannot be obtained here. These values are modified from the B-series propeller models (Oosterveld, et al., 1975).

$$\begin{aligned} K_T &= \sum_{i=1}^{39} C_{Ti} J^{s_i} \left(\frac{P}{D}\right)^{t_i} \left(\frac{A_E}{A_O}\right)^{u_i} z^{v_i} \\ &= a_1 J^2 + b_1 J + c_1 \end{aligned} \tag{24}$$

$$
\begin{aligned}
K_Q &= \sum_{i=1}^{47} C_{Qi} J^{s_i} \left(\frac{P}{D}\right)^{t_i} \left(\frac{A_E}{A_O}\right)^{u_i} z^{v_i} \\
&= a_2 J^2 + b_2 J + c_2
\end{aligned} \tag{25}
$$

where C_T, C_Q, s, t, u, and v are the coefficients obtained from model experiments of the B-series propeller, P is the pitch of the propeller, A_E/A_O is the ratio of propeller area, z is the number of blades of the propeller, and J is an advanced constant that is expressed as

$$
J = \frac{(1-w)V}{nD} \tag{26}
$$

where w is the wake fraction and V is the speed of the ship (m/s). Further, the coefficients a_1, b_1, c_1, d_1, a_2, b_2, c_2, and d_2 are obtained for each ship using the least squares method.

3.5. Evaluation of Speed Loss

The speed of the ship is determined using the relation between the propulsion forces and the resistance forces. The propulsion forces consist of the reduced thrust in waves, and the resistance forces are divided into the wave resistance in still water and the added resistance. In still water, ships must satisfy the following relationship between the thrust and the resistance:

$$
(1-t)T(V) = R_{SW}(V) \tag{27}
$$

where t is the thrust reduction factor due to mechanical loss. The relation is expressed as

$$
\begin{aligned}
\beta_{TV}(n,h)(1-t)T(V) &= R_{SW}(V) + R_{AW}(\omega,\chi,V) + R^A_{AW}(\omega,\chi,V) \\
&+ R_{WD}(U_W,\theta_W)
\end{aligned} \tag{28}
$$

When a ship sails in rough waves, the engine is usually controlled to prevent overload conditions. There are different types of engine controls, such as a constant speed control, constant revolution control, constant torque control, and constant power control. Constant speed control and constant revolution control do not seem to be realistic in rough waves; hence, they are not considered in this study. The other engine controls are modeled as follows (Hagiwara, et al., 2013):

$$
Q_B(n,V) - Q_E(n_E) = 0 \tag{29}
$$

$$
\begin{aligned}
&R_{SW}(V) + R_{AW}(\omega,\chi,V) + R^A_{AW}(\omega,\chi,V) + R_{WD}(U_W,\theta_W) \\
&-\beta_{TV}(n,h)(1-t)T(V) = 0
\end{aligned} \tag{30}
$$

$$2\pi n Q_B(n,V) - P_E(n_E) = 0 \tag{31}$$

$$R_{SW}(V) + R_{AW}(\omega,\chi,V) + R^A_{AW}(\omega,\chi,V) + R_{WD}(U_W,\theta_W) - \beta_{TV}(n,h)(1-t)T(V) = 0 \tag{32}$$

where Q_E is the engine torque, n_E is the engine revolution, P_0 is the power of the ship in still water, and P_E is the power of the main engine. Simultaneous equations (29) and (30) for constant torque control, and equations (31) and (32) for constant power control, must be satisfied if these engine controls are used at sea. The engine torque satisfies the following relation with the propeller torque (Bondarenko, et al., 2010):

$$2\pi I_p \frac{dn}{dt} = Q_E(n_E,h_E) - Q_B(n,V) \tag{33}$$

$$Q_E(n_E,h_E) = Q_{MCR}(n_{MCR},h_{MCR}) \left\{ 0.5 \left(\frac{h_E}{h_{MCR}}\right)^{2/3} + 1.5 \left(\frac{h_E}{h_{MCR}}\right)^{1/3} \left(\frac{n_E}{n_{MCR}}\right) - \left(\frac{n_E}{n_{MCR}}\right)^2 \right\} \tag{34}$$

where I_p is the inertia moment of the rotating parts in the propeller shaft plus mass and added mass moment of inertia of the propeller and h_E is the fuel oil consumption of the main engine (g/kW/h). Further, Q_{MCR}, n_{MCR}, and h_{MCR} are the engine torque, engine revolution, and fuel oil consumption at the maximum continuous rating (MCR). No reduction gear is installed for the 28,000DWT bulk carrier here, and the relation $n \sim n_E$ is satisfied. In constant torque control, the engine revolution and fuel injection are determined to equalize $Q_B(n,V)$ and $Q_E(n_E,h_E)$. They are automatically controlled in the governor by monitoring the engine loads or combustion. It is important to consider the detailed information of the fuel notch in numerical simulations. However, no such records or data are available in the engine log book, etc. The engine torque, engine power, and fuel oil consumption are estimated from the characteristic curve provided by the manufacturer. The characteristic curve on the fuel oil consumption is only shown if the engine power is larger than 2,000 kW. Eqs. (35) and (36) are only valid at $P_E \geq$ 2,000 kW.

$$P_E(n_E) = 2\pi n_E Q_E(n_E,h_E) = p_1 n_E^3 \quad (\text{for } P_E \geq 2,000\text{kW}) \tag{35}$$

$$h_E = p_2 P_E(n_E)^3 + p_3 P_E(n_E)^2 + p_4 P_E(n_E) + p_5 \quad (\text{for } P_E \geq 2,000\text{kW}) \tag{36}$$

The relation $n \sim n_E$ can be applied for the bulk carrier. Eq. (35) gives the estimation of the engine power, while Eq. (36) gives the estimation of the fuel oil consumption. If these estimated values are substituted into Eq. (35), the value of P_E can be finally determined. The coefficients p_1, p_2, p_3, p_4, and p_5 are defined from measured data by using the least squares method. The wave states are irregular in an actual sea, and the speed loss under irregular sea states must be considered. The longitudinal motion (speed of the ship) can be expressed as follows (Prpić-Oršić, et al., 2012):

$$(M + m_{11}(\omega_i)) \frac{dV}{dt} = T_T(H_i, \omega_i, \chi, V) - R_T(H_i, \omega_i, \chi, V) \tag{37}$$

$$\begin{aligned} T_T(H_i, \omega_i, \chi, V) &= \beta_{TV}(1-t)T(n, V) & (38) \\ R_T(H_i, \omega_i, \chi, V) &= R_{SW}(V) + R_{AW}(\omega, \chi, V) + R^A_{AW}(\omega, \chi, V) \\ &+ R_{WD}(U_W, \theta_W) & (39) \end{aligned}$$

where M is the mass of the ship, $m_{11}(\omega)$ is the added mass in surge mode at the i-th angular frequency in the time series of the wave, T_T is the total thrust, and R_T is the total resistance. The damping force connected with surge oscillatory motion is relatively small in the longitudinal direction and is hence ignored in this study. In an irregular sea state, Eq. (37) must be solved in the time domain. As shown in Figure 4, wave series have different amplitudes and periods for each component. Based on Hsu's assumption (Hsu, et al., 1970), the added resistance (wave drift force) in irregular waves can be approximated as a series of regular waves with different amplitudes and periods. Each regular wave is a combination of two neighboring waves of half wave length. The zero-up cross method is used to analyze the wave series. Eq. (37) is numerically solved using the fourth order Runge-Kutta method. Eqs. (29) $\sim$ (32) are considered in each step of the integration. Time series of irregular waves are regarded as the combination of different regular wave components. The added resistance is computed in the i-th different wave period, T_i, and height, H_i. The time step of numerical integration is defined as T_i, which varies in each wave of 2-16 s. Once the speed of the ship, V, is obtained, the thrust, torque, engine power, and fuel consumption can be determined simultaneously. To solve Eq. (37) with engine controls, numerical procedures are considered as follows. In constant torque control, Eq. (26) is transformed into a function of n, V, and h_E by substituting Eqs. (23), (25), and (34).

$$0.1\rho D^3 \left\{ a_2(1-w)^2 V^2 + D b_2 (1-w) V n + D^2 c_2 n^2 \right\} - Q_E(n_E, h_E) = 0 \tag{40}$$

Eq. (40) can be regarded as the second-order algebraic equation with an unknown variable n when we compute the value of $T_T(H_i, \omega_i, \chi, V)$.

$$\alpha_1 n^2 + \alpha_2 n + \alpha_3 = 0 \tag{41}$$

where the coefficients α_1, α_2, and α_3 are expressed as

$$\begin{aligned} \alpha_1 &= 0.1\rho D^5 c_2 \\ \alpha_2 &= 0.1\rho D^4 b_2 (1-w) V \\ \alpha_3 &= 0.1\rho D^3 a_2 (1-w)^2 V^2 - Q_E(n_E, h_E) \end{aligned} \tag{42}$$

Eq. (41) is solved by the iterative Newton-Raphson method, and the value of n is determined. As the relation $n_E \sim n$ is satisfied, the values of h_E and P_E are fixed by Eqs. (35) and (36). If the procedure is iterated in each time step, the speed loss can be analyzed in constant torque control. In constant power control, Eq. (29) is transformed into the third-order algebraic equation with unknown variable n.

$$\alpha_4 n^3 + \alpha_5 n^2 + \alpha_6 n + \alpha_7 = 0 \tag{43}$$

where the coefficients α_4, α_5, α_6, and α_7 are expressed as

$$\begin{aligned} \alpha_4 &= 2\pi\rho D^5 c_2 \\ \alpha_5 &= 2\pi\rho D^4 b_2 (1-w) V \\ \alpha_6 &= 2\pi\rho D^3 a_2 (1-w)^2 V^2 \\ \alpha_7 &= -P_E(n_E, h_E) \end{aligned} \tag{44}$$

Eq. (43) is solved using the same method as that for Eq. (41), and the value of n is obtained. The values of n_E, h_E, and P_E are obtained in each time step, and the speed loss can be analyzed in constant power control. Thus, the speed loss in an irregular sea state can be obtained to maintain constant values of torque or engine power. The revolution, thrust and engine power are simultaneously obtained in the time series analysis in Eq. (37). In the constant power control, they can obtained in Eqs. (43)(44) with Eq. (37).

4. Computed Results for Speed Loss

4.1. Computed Results of Added Resistance

Here, the speed loss is simulated and validated for the 28,000DWT bulk carrier in rough waves of the Southern Hemisphere. The main dimensions

of the ship are listed in Table 1, and the draft condition is half loaded. The offset of the ship is approximated from a similar model of a bulk carrier, as shown in Figure 5. The computed added resistances in three wave directions (0°, 30°, and 60°) are shown in Figure 6, which are obtained by the EUT and the NSM. The wave directions of 0°, 90°, and 180° are defined as bow (head sea state), beam (beam sea state), and stern (following sea state), respectively. The common non-dimensioned peak values are $4 \sim 17$ when the wave length, λ, is close to the ship length, L. On the other hand, the values for short wave lengths ($L/\lambda > 2$) are different in the EUT and the NSM. The NSM evaluates it to be below 0.5, whereas the EUT computes it as $1 \sim 4$. This factor may influence the evaluation of speed loss due to waves in the high frequency region. The computed results of the added resistance are shown in Figure 7 using the asymptotic formulas of Faltinsen and Okusu (Faltinsen, et al., 1980) (Okusu, 1986) in the three wave directions. The formula of Faltinsen evaluates it as $2 \sim 4$, whereas the formula of Okusu evaluates it as $2 \sim 6$, where $2 < L/\lambda < 8$. If these computed results are added to those of the NSM, they become relatively similar to those of the EUT. The influence of a short wave length is not significant for a container ship (slender shape) (Faltinsen, et al., 1980); however, asymptotic analysis must be considered for a bulk carrier if the NSM is used. The difference in speed loss in this regard will be discussed later.

4.2. Computed Results of Thrust and Resistance in Still Water

In Eqs. (21) and (22), the coefficients of the second-order polynomials are obtained as $a_1 = -0.146, b_1 = -0.2576, c_1 = 0.2929$ and $a_2 = -0.0196, b_2 = -0.0184, c_2 = 0.0309$, respectively. Figure 8 shows the estimated results of the thrust and torque coefficients, K_T and $K_{QB} = \eta_R K_Q$, and the resistance and thrust in still water for the 28,000DWT bulk carrier. The values of K_T and K_{QB} are $0 \sim 0.3$ and $0 \sim 0.03$, respectively. The resistance in still water, $R_{SW}(V)$, varies from 0 to 500 kN below a navigation speed of $14 \sim 15$ knots. The reduced thrust also varies from 400 to 600 kN, which implies that these empirical models can reproduce the measured values for the bulk carrier.

4.3. Computed Results of of Wind and Wave

The authors have already summarized detailed results for winds and waves using numerical simulation models and a meteorological database for Cases A and B (Lu, et al., 2017). As mentioned previously, three different

wind conditions are compared (see Table 2). NCEP-FNL contains global meteorological information provided by NCEP, and it covers every 1° and 6 h. The ERA interim contains global meteorological information from ECMWF, and it covers every 0.7° and 6 h. First, wind distributions are constructed every 0.5° as global (outer region) and every 0.1° as inner region where the ship is located. The linear interpolated wind conditions are also compared with the wind condition of the inner region computed by the WRF (The Weather and Research Forecasting) physical air model (Shamarock, et al., 2008). The wave conditions are numerically simulated for three wind conditions using the global model Wave WATCH III (WW3) (Tolman, 2002). A two-way nesting technique is applied at the boundary between the inner and outer regions. The measured and simulated results of wind directions and speeds for the ship in Cases A and B are shown in Figures 9 and 10. The simulated waves are compared with the waves measured by radar on the ship for Cases A and B, as shown in Figures 11 and 12. In Case A, there are differences of $1 \sim 3$ m in the wave height and -30 $\sim$ -60° from the ship's bow in the wave direction. The corresponding differences in Case B are 1 m and $0 \sim 60°$. The simulated results are obtained as a directional spectrum, and they can generate a time series of a wave as follows:

$$\eta(t) = \sum_{i=1}^{N} \sqrt{S(\omega_i)\Delta\omega}\cos(\omega_i t - \epsilon_i) \tag{45}$$

$$S(\omega) = \int_0^{2\pi} D(\omega, \theta_{WV}) d\theta \tag{46}$$

where $S(\omega)$ is the frequency spectrum of the waves, $D(\omega, \theta)$ is the directional spectrum of the waves obtained by the WW3 model, θ_{WV} is the true wave direction, t is the time, ϵ is the phase angle with random generation, and N is the number of wave components. The time period of a wave series is set to 3 h to maintain the stationary state of the wave series. The wave conditions for numerical simulations of speed loss are summarized in Tables 3 and 4.

4.4. Speed Loss in Irregular Waves

The speed loss is numerically analyzed for the simulated waves, as summarized in Tables 3 and 4. As shown in the previous section, the thrust of the ship decreases if the submergence of the propeller is insufficient because of relative vertical motion. The estimated values of the reduced thrust factor, β_{TV}, are shown for Cases A and B in Figure 13. The average values of

β_{TV} are 0.82 $\sim$ 0.86 with the EUT and 0.89 $\sim$ 0.93 with the NSM in Case A, while they are 0.69 $\sim$ 0.75 with the EUT and 0.75 $\sim$ 0.78 with the NSM. Estimated values of β_{TV} is larger in Case B. The EUT tends to estimate the thrust reduction factor to be 0.1 less than that estimated by the NSM.

The simulated speeds of the ship for Cases A-1-2, A-2-2, A-3-2, A-1-4, A-2-4, A-3-4, A-1-6, A-2-6, and A-3-6 are computed in two wave directions (30° and 60°) in Figures 14-16. In Figure 14, the speed loss of 2 $\sim$ 3 knots is simulated in each hindcasted wave and wave direction. There are very small differences among the four simulation methods of added resistance. On the other hand, the simulated speeds are different in each wave condition in Figures 15 and 16, when the wave heights are 4 $\sim$ 7 m. The speed is zero in some parts of these figures. Hence, the total resistance is larger than the thrust. In actual ships, engine power might be additionally applied to generate forward speed. This factor cannot be considered in the simulation of engine control. In particular, the speed loss becomes larger if the asymptotic formulas of added resistance are additionally considered. The speed is higher by 1 $\sim$ 4 knots in these cases, when the wave direction varies from 30° to 60°. The ship heading varies in this range of directions, and the measured value should exist between these wave directions. The significant wave height differs by 1 $\sim$ 3 m here, and it also leads to a difference of 4 $\sim$ 6 knots in speed. The simulated speeds of the ship for Cases B-1-7, B-2-7, B-3-7, B-1-8, B-2-8, and B-3-7 are computed for two wave directions (30° and 60°) in Figures 17 and 18. The speed loss is overestimated in Cases B-1-7 and B-1-8, which is based on the estimated wave using NCEP data. The authors have already shown that NCEP overestimates the actual situation (Lu, et al., 2017), and the result is the same in the case of speed loss. The other results are relatively similar, and the speed increases by 1 $\sim$ 2 knots when the wave direction varies from 30° to 60°. There are very small differences among the simulation methods of added resistance in these cases. The simulated engine revolutions are also compared for Cases A-1-6, A-2-6, A-3-6, B-1-8, and B-2-8 in Figures 19 and 20. The simulated results are 95 $\sim$ 105 rpm, which are in good agreement with the measured values in Figures 1 and 2. The average values of the ship's speed, engine revolution, and engine power are calculated and compared with the measured results in Cases A and B, as shown in Figures 21-26. It is obvious that the speed losses are overestimated in Case A-1 (NCEP) and Case A-3 (WRF) on 2 $\sim$ 3 days if the wave direction is 30°. The simulated results are in agreement within a difference of 1 knot for Case A-3 (WRF) in the wave direction of 60°. On

the other hand, the speed losses are overestimated in all the cases under Case B, especially in Case B-1 (NCEP). The same tendency is observed, i.e., the ship's speed differs at wave directions of 30° and 60° in Cases B-1 and B-3. There are small differences in the ship's speeds in each model of added resistance. However, the simulated speeds differ significantly if the wave direction is 30°, i.e., in a head sea state. The speed loss becomes larger when asymptotic models are additionally considered with the NSM. The estimated values are closer if the wave direction is 60° rather than 30° in Figures 21 and 22. The same tendency can be seen in the average revolutions. In Figure 23, the simulated revolutions are larger for 5 rpm in Case A. On the other hand, they are slightly smaller by $1 \sim 2$ rpm in Case B, as shown in Figure 24. The engine power is underestimated if the wave direction is 30° in Case A, and it agrees within 100 kW when the direction is 60°. It is not necessarily in agreement in the entire period in Case B, because the ship increases the engine power at $1 \sim 1.5$ days, as shown in Figure 26. These results indicate that the differences in weather simulations and wave direction have a greater influence on the speed loss than those of seakeeping models.

4.5. Estimation of Fuel Consumption and CO_2 Emission

The accuracy of estimation is validated for two rough sea voyages here, and the magnitude of error can be shown. The fuel oil consumption is one of the most important factors in the optimal ship routing, and is compared in each case. As shown in Eq. (36), the fuel consumption can be estimated from the third-order polynomial provided by its manufacturer. The gauge of fuel oil tank is also monitored in the measurement, and total consumption of fuel oil is available as the difference of gauge values. However, it contains components of fuel consumed by other auxiliary machines or generators, besides the main engine. The consumed volume of fuel oil, h_{EV}, is obtained as

$$h_{EV} = \frac{h_E P_E(n_E)}{\rho_{oil} \times 1000} \tag{47}$$

where ρ_{oil} is the density of fuel oil, which is defined here as 0.952 kg/ℓ. The coefficients in Eqs. (35) and (36) are obtained as $p_1 = 0.281 \times 10^{-2}, p_2 = 0.1 \times 10^{-9}, p_3 = -0.9 \times 10^{-6}, p_4 = -0.6 \times 10^{-3}$, and $p_4 = 183.68$. The consumed volume of fuel oil in Eq. (47) is compared with the volume in the fuel oil tank for Cases A and B, as shown in Figure 27. It is obvious that the measured values are equally larger than those in Eq. (47). The calculated root mean square values are 85.36 and 83.24 ℓ/h, respectively. It seems

reasonable to assume that fuel oil of 80 $\sim$ 85 ℓ/h is consumed in auxiliary machines, generators, etc. The consumed volume in Eq. (47) should be used for comparison with the estimated results in Cases A and B. The estimated results of fuel oil consumption are compared for two wave directions (30° and 60°) in Cases A and B, as shown in Figures 28 -29. There are small differences in the fuel oil consumption in each simulation method of added resistance in Cases A and B. However, in Case B, the simulated values are 70 $\sim$ 80 ℓ smaller (1.5 $\sim$ 2 days) than the actual ones. The ship increases the engine power during this period, and the engine power is set to a constant value in the numerical simulation. This factor might influence the underestimation, as shown in Figure 29. The CO_2 emission is also briefly estimated here and compared among the simulated results. A simple relation between the gas emission and the fuel oil consumption is proposed as follows.

$$CO_2 = \rho_{oil} h_{EV} \times GEF \tag{48}$$

where GEF is the gas emission factor based on mass (3.173 kg of CO_2 emission per kg of fuel oil). The fuel oil consumption and CO_2 emission are totally evaluated during the period in each simulation case, i.e., 45 h in Case A and 33 h in Case B. The total fuel oil consumption and CO_2 emission during the period are calculated as

$$h_{ET} = \sum_{i=1}^{N} h_{EVi} \Delta t_i \tag{49}$$

$$CO_{2T} = \sum_{i=1}^{N} CO_{2i} \Delta t_i \tag{50}$$

where h_{ET} is the total fuel oil consumption during the simulation period, CO_{2T} is the total CO_2 emission during the simulation period, Δt_i is the time interval between the i-th and (i+1)-th simulation points, and N is the number of simulated points ($N = 9$). As shown in the previous section, the ship's speed decreases significantly and the sailing distance varies in each weather condition. These parameters should be evaluated as values per nautical mile. The sailing distance during the period is obtained as

$$D_T = \sum_{i=1}^{N} V_i \Delta t_i \tag{51}$$

The fuel oil consumption and CO_2 emission per nautical mile are expressed as follows:

$$h_{EM} = \frac{h_{ET}}{D_T} \tag{52}$$

$$CO_{2M} = \frac{CO_{2T}}{D_T} \tag{53}$$

The computed results of these parameters, h_{EM} and CO_{2M}, are compared with the measured results in Cases A and B with two wave directions of 30° and 60°, as shown in Figures 30-33. In Cases A, the fuel oil consumption differs by $10 \sim 40$ ℓ per nautical mile in the wave direction of 30°. The differences in the ship's speed contribute to this result. On the other hand, there are small differences if the wave height is 60°. In Case B, the difference in fuel oil consumption is $10 \sim 20$ ℓ per nautical mile, which is less than that in Case A. The same result is obtained, i.e., the differences are small in each wave condition and numerical model of added resistance, if the wave direction is 60°. These patterns of differences are common in the evaluated values of CO_2 emission per nautical mile, as shown in Figures 32 and 33. The range of variation is $20 \sim 100$ kg per nautical mile in Case A and $20 \sim 50$ kg per nautical mile in Case B. However, the difference is less than 30 kg per nautical mile when the wave direction is 60°. The wave direction is simulated as $30 \sim 60°$, which varies in both cases. It has already been shown that the heading of the ship tends to vary more frequently in rough seas than in calm seas (Lu, et al., 2017). The speed loss should be evaluated by combining the simulated results in multiple wave directions, such as $30 \sim 60°$ here.

5. Conclusions

This study focused on changes in a ship's performance in rough sea voyages, and comparisons were made against measured results for a 28,000DWT bulk carrier in the Southern Hemisphere. The accuracy was validated for each practical simulation model of added resistance. The main conclusions can be summarized as follows.

(1) Three remarkable speed losses were measured in the Southern Hemisphere, and two of them seemed to be similar situations of the main engine. The power of the main engine showed a relatively constant value, although the ship's speed and engine revolutions were reduced significantly. These rough sea voyages were analyzed by approximation as constant power control of main engine.

(2) Although there are various estimation methods of the added resistance, four patterns were compared with each other. It is known that added resistance exists at $L/\lambda > 2.0$ because of the blunt shape of the ship. The NSM underestimates it, and it is reasonable to add the diffraction component of asymptotic formulas. The EUT can compute it accurately, and is not necessary to consider asymptotic formulas additionally.
(3) Thrust reduction factors were computed for simulated results of waves in rough sea navigations. They were found to vary with the wave condition, wave direction, and ship's speed, and the values were $0.6 \sim 1.0$. The average values of the EUT were $0.05 \sim 0.1$ smaller than those of the NSM. The total thrust was smaller when the relative vertical motion was evaluated by the EUT under rough sea conditions.
(4) The ship's speed in irregular waves was compared for each added resistance method, wave direction, and simulated wave in two rough sea voyages. There were small differences among the simulation methods if the significant wave height was less than $2 \sim 2.5$ m. On the other hand, the simulated ship's speeds were significantly different for each method, especially at a wave direction of 30°. It became zero in Case A-3-6, because the simulation was carried out as constant power control. Ships are found to increase the engine power in this situation from measured data; deliberate speed loss under human factors becomes necessary in extreme wave conditions. The estimated results of revolutions of the main engine have a similar tendency.
(5) The ship's average speeds were $5 \sim 6$ knots smaller in Cases A and B if the simulated wave conditions were overestimated by $2 \sim 3$ m at a wave direction of 30°. This result verifies the reasonability of wave estimation in the authors' previous study (Lu, et al., 2017). The difference was smaller when the wave direction was defined as 60° because the added resistance was smaller.
(6) The condition setting of the time series (spectrum) for the estimated waves and wave direction was found to influence the accuracy of speed loss rather than the difference in the simulation models for added resistance. In other words, considerable uncertainty remains in the estimation of rough waves in the Southern Hemisphere.
(7) The speed loss was numerically evaluated under the theory of constant power control for Cases A and B, and the simulated results of engine power decreased by $100 \sim 200$ kW as the wave condition became more severe. This might be attributed to the increased added resistance. The measured results showed that the ship generates extra engine power of $200 \sim 300$ kW in Cases

A and B. This factor cannot be considered in this study, and it is necessary to adopt an algorithm for the deliberate speed loss.
(8) The fuel oil consumption was compared in each case per nautical mile. They were 90 and 70 ℓ per nautical mile, estimated by Eq. (44), in Cases A and B, respectively. This implies that the magnitude of speed loss strongly influences the values of fuel oil consumption, e.g., there is a difference of 20 ℓ per nautical mile. Moreover, the uncertainty in weather estimation leads to an additional error of $10 \sim 20$ ℓ, especially at the head sea state of $0 \sim 30°$. There are small differences in each weather condition and simulation method at the oblique sea state of $30 \sim 60°$.
(9) The emission of CO_2 was estimated as $220 \sim 260$ kg per nautical mile in rough seas for $4 \sim 7$ m of significant wave height, especially in Cases A-3 (WRF) and B-1 (NCEP). It could vary by $50 \sim 100$ ℓ per nautical mile at a wave direction of 30°. Further, the differences were smaller (within 30 kg per nautical mile) at a wave direction of 60°. The speed loss should be evaluated by combining the simulated results in multiple wave directions from head sea to oblique sea states.

Acknowledgement

The authors wish to extend their gratitude to Shoei Kisen Kaisha, Ltd., for their cooperation in conducting onboard measurements of the 28,000DWT bulk carrier for six years. Further, we wish to express our appreciation for the ship crews and local agencies for their insightful advice during the onboard measurement. In addition, we would like to thank Dr. Renato Skejic, MARINTEK, Norway, for his guidance in evaluating marine engines. This study was conducted as "The International Collaboration on Strongly Nonlinear Fluid Structure Interactions and Nurturing Young Researchers in Ocean Engineering" ($2012 \sim 2014$, represented by Prof. Masashi Kashiwagi), Japan Society for the Promotion of Science (JSPS). This study was financially supported by Scientific Research (B) ($2012 \sim 2015$ and $2016 \sim 2018$, represented by Kenji Sasa) and Challenging Explanatory Research ($2015 \sim 2017$, represented by Kenji Sasa) under Grants-in-Aid for Scientific Research, JSPS. This study was also supported by the Croatian Science Foundation - project 8722 and the University of Rijeka (contract no. 13.09.1.1.05).

References

Bondarenko, O. and Kashiwagi, M., "Dynamic behavior of ship propulsion

plant in actual seas", *Journal of Japan Institute of Marine Engineering*, *Vol.45*, pp.1012-1016, 2010

Bondarenko, O. and Kashiwagi, M., "Statistical consideration of propeller load fluctuation at racing condition in irregular waves", *Journal of Marine Science and Techology*, *Vol.16*, pp.402-410, 2011

Butterworth, J., Atlar, M. and Shi, W., "Experimental analysis of an air cavity concept applied on a ship hull to improve the hull resistance", *J. Ocean Engineering*, *Vol.110*, *Part B*, pp.2-10, 2015

Dee, D. P., et al., "The ERA-interim reanalysis, configuration and performance of the data assimilation system", *Q. J. R. Meteorol. Soc.*, *Vol.137*, *No.656*, pp.553-597, 2011

Devanney, J., "The impact of the energy efficiency design index on very large VLCC design and CO2 emissions", *Ship and Offshore Structures*, *Vol.6*, *No.4*, pp.355-368, 2011

Faltinsen, O.M., "Sea loads on ships and offshore structures", *Cambridge University Press*, 328p., 1993

Faltinsen, O.M., Minsaas, K.J., Liapis, N. and Skjørdal, S., "Prediction of resistance and propulsion of a ship in a seaway", *Proceedings of the 13th Symposium on Naval Hydrodynamics*, pp.505-529, 1980

Fujino, M. and Sakurai, K., "On the evaluation of wave exciting roll moment by the strip method", *Journal of the Society of Naval Architects of Japan*, *Vol.152*, pp.125-137, 1982 (in Japanese)

Fujiwara, T., Ueno, M. and Nimura, T., "Estimation of wind forces and moments acting on ships", *Journal of the Society of Naval Architects of Japan*, *Vol.183*, pp.77-90, 1998 (in Japanese)

Hagiwara, S., Yamasaki, S., Yoshimura, Y. and Adachi, H., "Ship performance design", *Seizando Shoten*, 255p., 2013 (in Japanese)

Hanaoka, T., "Theoretical study on ship motions in head sea", *Collection of Papers of Dr. Tatsuro Hanaoka*, pp.53-107, 1976 (in Japanese)

Hanssen, G.L. and James, R.W., "Optimum ship routing", *The Journal of the Insititute of Navigation*, *Vol.13*, *No.3*, pp.253-272, 1960

Holtrop, J.A., "A statistical re-analysis of resistance and propulsion data", *Proceedings of the International Shipping Progress*, *Vol. 31*, pp.272-276, 1984

Holtrop, J.A. and Mennen, G.G.J., "An approximate power prediction method", *Proceedings of the International Shipping Progress*, *Vol. 29*, pp.166-170, 1982

Hsu, F.H. and Blenkarn, K.A., "Analysis of peak mooring force caused by slow vessel drift oscillation in random seas", *Proceedings of Ocean Technology Conference(OTC)*, *Vol.1*, pp.135-146, 1970

Kalnay, E., et al., "The NCEP/NCAR 40-year reanalysis project", *Bulletin of American Meteorology Society*, *Vol.77*, *No.3*, pp.437-471, 1996

Kashiwagi, M., "Calculation formulas for the wave-induced steady horizontal force and yaw moment on a ship with forward speed", *Reports of Research Institute for Applied Mechanics, Kyushu University*, *Vol.37*, *No.107*, pp.1-18, 1991

Kashiwagi, M., "Added resistance, wave-induced steady sway force and yaw moment on an advancing ship", *Ship Technology Research*, *Vol.39*, pp.3-16, 1992

Kashiwagi, M., Sugimoto, K., Ueda, T., Yamasaki, K., Arihama, K., Kimura, K. Yamashita, R., Ito, A. and Mizokami, S., "An analysis system for propulsive performance in waves", *Journal of Kansai Society of Naval Architect, Japan*, *No. 241*, pp.1-16, 2004 (in Japanese)

Kosmas, O.T. and Vlachos, D.S., "Simulated annealing for optimal ship routing", *Computers and Operations Research*, *Vol.39*, pp.576-581, 2012

Lin, Y.H., Fang, M.C. and Yeung, R.W., "The optimization of ship weather-routing algorithm based on the composite influence of multi-dynamic elements", *J. Applied Ocean Research*, *Vol.43*, pp.184-194, 2013

Lu, L.F., Sasa, K., Sasaki, W., Terada, D., Kano, T. and Mizojiri, T., "Rough wave simulation and validation using onboard ship motion data in the Southern Hemisphere to enhance ship weather routing", *J. Ocean Engineering* (Under Review)

Maki, A., Akimoto, Y., Nagata, Y., Kobayashi, S., Kobayashi, E., Shiotani, S., Ohsawa, T. and Umeda, N., "A new weather-routing system that accounts for ship stability based on a real-coded genetic algorithm", *Journal of Marine Science and Technology*, *Vol.16*, pp.311-322, 2011

Newman, J.N., "The theory of ship motions", *J. Advances in Applied Mechanics*, *Vol.18*, pp.221-283.

NYK (Nippon Yusen Kaisha), "NYK super eco ship 2030", *http://www.nyk.com/english/csr/envi/ecoship/*, 2009

Okusu, M., "Added resistance of blunt bow ships in very short waves", *Journal of Kansai Society of Naval Architect, Japan*, *No. 202*, pp.39-42, 1986

Oosterveld, M.W.C. and Van Oossanen, P., "Further computer-analyzed data of the Wageningen B-screw series", *Proceedings of International Shipping Progress*, *Vol.22*, *No.251*, pp.3-14, 1975

Prpić-Oršić, J. and Faltinsen, O.M., "Estimation of speed loss and associated CO2 emissions in a seaway", *J. Ocean Engineering*, *Vol. 44*, pp.1-10, 2012

Salvesen, N., Tuck, E.O., Faltinsen, O.M., "Ship motions and sea loads", *Transaction of the Society of Naval Architects and Marine Engineers*, *No.6*, pp.1-30, 1970

Skamarock, W. C., Klemp, J. B., Dudhia, J., Gill, D. O., Barker, D. M., Duda, M. G., Huang, X.-Y., Wang, W. and Powers, J. G., "A description of the advanced research WRF version 3., *NCAR Technical Note NCAR/TN-475+STR*, 113p., 2008

Smogeli, O.N., "Control of marine propellers from normal to extreme conditions", *Ph.D Thesis of Dept. of Marine Engineering and Science, NTNU*, 242p., 2006

Tolman, H.L., "Validation of WAVEWATCH III version 1.15 for a global domain", *NOAA/NWS/NCEP/OMB Technical Note*, *Nr. 213*, 33p., 2002

Vettor, R. and Guedes Soares, C., "Rough weather avoidance effect on the wave climate experienced by oceangoing vessels", *J. Applied Ocean Research*, *Vol.59*, pp.605-615, 2016

Yasuda, E., Iwashita, H. and Kashiwagi, M., "Improvement of Rankine panel method for seakeeping prediction of a ship in low frequency region", *Proceedings of the 35th International Conference on Ocean, Offshore and Arctic Engineering*, pp.1-9, 2016

Development and validation of speed loss for a blunt-shaped ship in two rough sea voyages in the Southern Hemisphere

Kenji Sasa[1,*]

5-1-1, Fukae Minami Machi, Higashinada-ku, Kobe, 658-0022 JAPAN

Odd Magnus Faltinsen[2], Li-Feng Lu[1], Wataru Sasaki[3], Jasna Prpić-Oršić[4], Masashi Kashiwagi[5], Takuro Ikebuchi[6]

Abstract

Maritime transportation is becoming increasingly complex owing to the fluctuation of oil prices, the introduction of environmental guidelines, and the onset of climate change. Although optimal routing has been researched for decades, few studies have investigated speed loss in rough waves for ships with blunt shape and low speed. Onboard measurement of a 28,000DWT bulk carrier has been conducted for six years in rough sea voyages in the Southern Hemisphere. It is necessary to validate the wave and wind conditions in order to discuss speed loss in these situations. Here, numerical simulation of speed loss is developed and conducted for each estimated wave condition. The speed losses under different numerical models of added resistance are quantitatively compared in two rough sea voyages. The simulated results of speed loss are in good agreement with the measured results if the

*Corresponding Author
Email address: sasa@maritime.kobe-u.ac.jp (Kenji Sasa)
[1]Dept. of Maritime Sciences, Kobe University
[2]Centre for Autonomous Marine Operations and Systems, Norwegian University of Science and Technology
[3]Wind Energy Institute of Tokyo, Inc. (Japan Agency for Marine-Earth Science and Technology)
[4]Faculty of Engineering, University of Rijeka
[5]Dept. of Naval Architecture and Ocean Engineering, Osaka University
[6]Imabari Shipbuilding Co., Ltd.

estimated wave is accurate and the wave direction is properly defined. The speed loss accuracy is significantly influenced by the wave estimation accuracy or wave direction setting compared to that in the numerical models of added resistance in actual seas. Simulated results provide important information to evaluate the performance of a ship with blunt shape in rough waves.

Keywords: Speed loss, added resistance, wave estimation, engine control, fuel oil consumption, gas emission, numerical simulation

1. Introduction

Optimal ship operation is one of the most important objectives in the maritime industry. Numerous studies have investigated various evaluation methods for optimal ship routing in previous decades (Hanssen, et al., 1960) (Maki, et al., 2011) (Komas, et al., 2012) (Lin, et al., 2013). Some objective functions for optimal routing, such as safety, voyage time, and fuel oil consumption, vary with the demand or circumstances in a particular era. Since the Energy Efficiency Design Index (EEDI) was introduced in 2012, gas emission has emerged as a major concern (Prpić-Oršić, et al., 2012). Various studies have investigated the optimization of the ship shape, main engine, and propellers (Devanney, 2011) (Butterworth, et al., 2015). To minimize gas emission and fuel oil consumption, the concept of a future ship, namely "Eco ship 2030", has been proposed (NYK, 2009). Optimal ship routing encompasses many fields, such as weather forecasting, seakeeping, propulsion, and machinery. A seafarer's intuition or experience is not sufficient to meet the requirements of optimal ship routing in terms of ship design and operation. Major meteorological organizations, such as the National Centers for Environmental Prediction (NCEP) (Kalnay, et al., 1996) and the European Centre for Medium-Range Weather Forecasts (ECMWF) (Dee, et. al., 2011), provide a downloadable global weather database. This database has been employed in various fields to determine the weather conditions and thus achieve reliable optimal ship routing in the Northern Hemisphere (Vettor, et al., 2016). However, the reliability of optimal routing in the Southern Hemisphere has not been investigated extensively thus far. The authors have already demonstrated the accuracy of wave estimation for three cases of rough sea voyages in the Southern Hemisphere using measured data of a 28,000DWT-class bulk carrier through numerical wind and

wave simulations (Lu, et al., 2017). It has been shown that the simulated winds are not necessarily in agreement with the measured ones. In particular, wind speed differences of 3 $\sim$ 10 m/s and wave height differences of 1 $\sim$ 3 m might exist between the NCEP and the ECMWF data for simulations in the Southern Hemisphere. In previous decades, many studies have investigated the added resistance and relative motion of vessels in the field of seakeeping (Faltinsen, 1993). Three-dimensional methods continue to suffer from problems in practical applications (Yasuda, et al., 2016), while time-domain methods involve a long computation time. Therefore, the strip theory remains the main method for evaluating the ship response and added resistance for optimal routing (Prpić-Oršić, et al., 2012). On the other hand, unified theories have been derived from the strip theory (Newman, 1978). Kashiwagi et al. proposed the Research Initiative on Oceangoing Ships (RIOS), which is a novel system for evaluating ship performance in actual seas (Kashiwagi, et al., 2004). The seakeeping part of this system is based on the enhanced unified theory (EUT) (Kashiwagi, 1992). This method considers the three-dimensional problem in the outer region, and the solution is obtained by matching the outer solution with the inner solution obtained for a two-dimensional problem. The computed results have been shown to be nearly identical to the results of model tests. Speed loss of a ship can be modeled in combination with propulsion and machinery models (Faltinsen, et al., 1980) (Bondarenko, et al., 2011). Although many studies have estimated speed loss in a seaway, few have compared their results with measurements made in actual seas. Moreover, few studies have compared the strip method and EUT in terms of the total speed loss in a seaway. In the present study, these aspects are examined using the measured data of a bulk carrier in rough sea voyages in the Southern Hemisphere on the basis of the relation between the total thrust and the resistance. Remarkable speed losses are measured owing to extremely rough wave conditions (5 $\sim$ 7 m). Further, various parameters are analyzed to evaluate the speed loss in irregular waves with the ventilation of the propeller. Speed losses in two rough sea voyages are simulated considering different wave conditions and seakeeping models. Finally, the overall accuracy is evaluated on the basis of the ship's speed, engine power, CO_2 emission, etc., for vessels with blunt shape and low speed in rough seas of the Southern Hemisphere.

2. Onboard Measurement of Ship Performance

Techniques for monitoring ships in actual seas have been developed in recent decades. Owing to the development of network technologies, onshore monitoring of ships is becoming increasingly common. However, most of the information collected by these techniques is confidential and hence scarcely available. Moreover, there are not many examples of ships with blunt ship shape and low speed. Onboard measurement of the performance of a 28,000DWT class bulk carrier was underway for six years from July 2010 to August 2016 (Lu, et al., 2017). The ship is a tramper without regular routes. The management company changed in 2012, and there have been some changes in the navigation routes, engine operations, etc., since then. In particular, the main routes have been defined between Asian countries and locations in the Southern Hemisphere, such as Oceania or South America, after the change in ship management. The sea conditions in the Southern Hemisphere are believed to be rougher than those in the Northern Hemisphere, because the former has fewer landmasses. The authors have shown that remarkable difficulties were encountered during voyages in the Tasman Sea and the Atlantic Ocean as well as off the coasts of South Africa and Australia in 2013 $\sim$ 2016. The main dimensions of the ship are listed in Table 1. In this study, speed losses are discussed for the measurements made in the Southern Hemisphere. Figures 1 and 2 show the measured parameters, including the ship's motion, speed, engine revolution, engine power, fuel oil consumption, and exhaust gas temperatures on six cylinders of the main engine, on June 1 $\sim$ 4 (Case A) and June 14 $\sim$ 16 (Case B), 2013. Ship motion is expressed as significant values obtained by the zero-up cross method for a 10-min time series every 0.1 s. Other parameters are shown as averaged values for a 10-min time series every 1 s. Some of the tendencies can be summarized as follows.

(1) Very large ship motion, i.e., 15° of roll and 5° of pitch, occurred in rough sea conditions.

(2) Very strong wind speeds were measured in Case A (around 15 $\sim$ 25 m/s) for two days. Relatively strong wind speeds were measured in Case B (around 10 $\sim$ 20 m/s).

(3) Remarkable speed losses occurred in each case. In particular, the ship's speed reached a minimum value of 2 $\sim$ 3 knots in Case A. Thus, the ship nearly lost all its propulsion force against the total resistance in rough seas. The engine revolutions were reduced simultaneously from 109 rpm to 90 $\sim$

100 rpm over 10 min on average.
(4) The engine power, thrust, and fuel oil consumption were nearly constant in Cases A and B despite remarkable reduction in the ship's speed and engine revolution. It was assumed that the ship resistance prevents the ship from moving forward, even if propulsion force is supplied from the main engine. The engine control can be regarded as constant power control (or constant torque control) in Cases A and B.
(5) The exhaust gas temperature is one of the important factors affecting the intentional engine operation in rough sea voyages. The average temperature was 340 $\sim$ 380 C in all the cases. The temperature in one of the cylinders showed the highest values (around 370 $\sim$ 380 C). These values were nearly equal to those under 85% to 100% load condition in the test run. This implies that the main engine could be overloaded in such rough sea voyages. There is a possibility that the revolution (or injection of fuel oil) was manually controlled to not exceed an exhaust gas temperature of 370 C. The speed losses were numerically simulated for Cases A and B, which can be regarded as cases of constant power control of the main engine.

3. Estimation Method of Speed Loss

A ship's speed is determined by the relation between its thrust and resistance. A seaway presents different types of resistance, both in still water and in waves. The former is defined as the resistance in still water, and the latter is defined as the added resistance. The following subsections briefly describe numerical methods for reproducing each force related to speed loss analysis.

3.1. Ship Resistance in Still Water

Various resistance forces act on a ship, and they increase with the ship's forward speed, V. A ship's resistance in still water is expressed as

$$R_{SW}(V) = (1+k_1)R_F(V) + R_W(V) + R_{APP}(V) + R_B(V) + R_{TR}(V) + R_A(V) \tag{1}$$

where R_{SW} is the total resistance in still water, R_F is the resistance due to friction, R_W denotes the wave-making and wave-breaking resistance, R_{APP} is the resistance of the ship's appendages, R_B is the additional pressure resistance of the bulbous bow near the water surface, R_{TR} is the additional pressure resistance of the immersed transom stern, R_A is the model-ship

correlation resistance, and $(1 + k_1)$ is the form factor describing the viscous resistance of the hull in relation to R_F. In this study, the empirical method is used (Holtrop, et al., 1982) (Holtrop, 1984). It is difficult to estimate the form factor by using the potential theory because it includes a strong viscous component. Some formulas have been proposed. Here, we use the formula proposed by MARINTEK, which is expressed as

$$1 + k_1 = 1 + 0.6\gamma + 75\gamma^3 \tag{2}$$

$$\gamma = \frac{C_b}{L_{pp}}\sqrt{(d_F + d_A)B} \tag{3}$$

where C_b is the block coefficient, and d_F and d_A are the forward and aft perpendicular drafts. The viscous component, $R_F(V)$, is modeled as

$$R_F(V) = \frac{1}{2}\rho S V^2 C_F \tag{4}$$

where ρ is the water density, S is the wetted area of the ship, and C_F is the coefficient of frictional resistance, which is calculated by the formula proposed by ITTC (International Towing Tank Committee), where the roughness of the ship hull, ΔC_F, is given by

$$C_F = C_{F,ITTC} + \Delta C_F \tag{5}$$

$$C_{F,ITTC} = \frac{0.075}{(\log_{10} R_n - 2)^2} \tag{6}$$

$$\Delta C_F = \left\{111\left(AHR \cdot V\right)^{0.21} - 404\right\}\left(\frac{0.075}{(\log_{10} R_n - 2)^2}\right)^2 \tag{7}$$

where R_n is the Reynold's number shown in Eq. (8), and AHR is the averaged surface roughness of the ship hull ($75 \sim 150\ \mu m$).

$$R_n = V \times \frac{L}{\nu} \tag{8}$$

where, L is the ship's length and ν is the dynamic coefficient of viscosity ($=10^{-6}\mathrm{m}^2/\mathrm{s}$).

3.2. Estimation of Added Resistance

Two types of methods are used to estimate the added resistance. One is the pressure integration method for a ship in waves. Here, the conservation of momentum following Maruo's theory is used (Kashiwagi, 1991). The added resistance is calculated as

$$\begin{aligned}\frac{R_{AW}(\omega,\chi,V)}{\rho g\zeta^2} &= \frac{1}{4\pi k_0}\left[-\int_{-\infty}^{k_1}+\int_{k_2}^{k_3}+\int_{k_4}^{\infty}\right]\left\{|H_C(k)|^2+|H_S(k)|^2\right\} \\ &\times \frac{\kappa(k,V)\left\{k-k_0\cos(\chi-\pi)\right\}}{\sqrt{\kappa^2(k,V)-k^2}}dk \end{aligned} \tag{9}$$

where R_{AW} is the added resistance in waves, ω is the circular frequency, χ is the relative wave direction (0° is defined as ship bow), ρ is the water density, g is the acceleration due to gravity, ζ is the wave amplitude, k_0 is the wave number of the incident wave, and $H_C(k)$ and $H_S(k)$ are the Kochin functions that correspond to the symmetric mode and asymmetric mode, respectively. Further, $\kappa(k)$ is expressed as

$$\kappa(k,V)=\frac{1}{g}(\omega+kV)^2=K+2k\tau+\frac{k^2}{K_0} \tag{10}$$

$$K=\frac{\omega^2}{g},\quad \tau=\frac{V\omega}{g},\quad K_0=\frac{g}{V^2} \tag{11}$$

where τ is the Hanaoka parameter (Hanaoka, 1976). In addition, k_1, k_2, k_3, and k_4 are the wave numbers of the k_1 and k_2 wave systems, expressed as

$$\left.\begin{matrix}k_1\\k_2\end{matrix}\right\}=-\frac{K_0}{2}\left(1+2\tau\pm\sqrt{1+4\tau}\right) \tag{12}$$

$$\left.\begin{matrix}k_3\\k_4\end{matrix}\right\}=-\frac{K_0}{2}\left(1-2\tau\mp\sqrt{1-4\tau}\right) \tag{13}$$

The two Kochin functions are obtained from the EUT and the new strip method (NSM) (Salvessen, et al., 1970) (Fujino, et al., 1982). In the EUT, the Kochin function is obtained from the source strength and the doublet in the outer problem. This is described in detail in (Kashiwagi, 1992). It can be obtained using a similar technique in the NSM. The diffraction component

of the added resistance for a short wave length cannot be ignored for blunt-shaped ships, and two formulas are considered in the high frequency region (Faltinsen, et al., 1980) (Okusu, 1986). They are expressed as

$$\frac{R_{AW}^{A}(\omega,\chi,V)}{\rho g\zeta^{2}} = \frac{1}{2}\int_{L}\left\{\sin^{2}(\theta+\chi)+\frac{2\omega_{0}V}{g}\left(1-\cos\theta\cos(\theta+\chi)\right)\right\}n_{1}d\ell \tag{14}$$

$$\frac{R_{AW}^{A}(\omega,\chi,V)}{\rho g\zeta^{2}} = \frac{1}{2}\left(1+\frac{2\omega_{0}V}{g}\right)\int_{-B/2}^{B/2}\frac{K_{1n}}{k_{0}}n_{1}dy \tag{15}$$

$$K_{1n} = \frac{\left(\omega_{e}-k_{0}V\cos^{2}\theta\right)^{2}}{g}\sin(\varphi-\theta) \tag{16}$$

where R_{AW}^{A} is the added resistance as the diffraction component in the high frequency region, θ is the angle between the longitudinal line and the tangential line at the water line of ship, φ is the angle between the reflected wave and the ship's hull, n_1 is the normal vector in longitudinal direction at the calculation point, and ω_e is the encounter frequency. The added resistance due to wind is expressed as

$$R_{WD}(U_{W},\theta_{W}) = \frac{1}{2}\rho_{a}C_{X}(\theta_{W})A_{X}U_{W}^{2} \tag{17}$$

where ρ_a is the air density, C_X is the coefficient of wind resistance in the longitudinal direction, A_X is the front wind area, θ_W is the wind direction and U_W is the wind speed. Further, C_X is defined by Fujiwara's method (Fujiwara, et al., 1998).

3.3. Estimation of Deducted Thrust

If a ship's motion increases in waves, the relative surface elevations around the ship will vary. Therefore, the propeller must be sufficiently submerged in the water to generate propulsion force. However, the propeller sometimes emerges from the water because of the relative surface elevation. This causes a reduction in the propulsion force, which is called ventilation. Studies on the thrust reduction in waves have been conducted (Faltinsen, et al., 1980). Smogeli expressed it as a function of the propeller speed and the vertical distance between the propeller and the water surface (Smogeli, 2006). Figure 3 shows the thrust reduction function, β_{TV}, for an open propeller. In the

present study, the thrust reduction is modeled as a combination of the linear functions of propeller speed and relative surface elevation as follows:

$$\beta_{TV}(n,h) = f(n/n_{bp}, h/R) \tag{18}$$

where n is the propeller speed, n_{bp} is the bollard pull speed of the propeller, h is the vertical distance between the propeller and the water surface, and R is the radius of the propeller. The relative surface elevation at the position of the propeller, $\zeta_r(x_p)$, is required to obtain the value of h as follows:

$$h = h_p + \zeta_r(x_p) \tag{19}$$

$$\zeta_r(x_p) = \xi_3 + y_P\xi_4 - x_P\xi_5 - \varphi_0 \tag{20}$$

where h_P is the depth of the propeller in still water, $\xi_i (i = 3, 4, 5)$ represents the motion amplitudes for heave, roll, and pitch according to the EUT and the NSM, and φ_0 is the velocity potential of the incident waves. Thus, the thrust reduction factor, β_{TV}, can be obtained by Eq. (18).

3.4. Ship Thrust in Still Water

The propulsion force is also important for evaluating the speed loss, and it is estimated on the basis of the experimental results for the B-series propeller in open water (Oosterveld, et al., 1975). The thrust and torque coefficients are expressed as polynomials, and the thrust and torque of a ship are expressed as

$$T(n,V) = \rho n^2 D^4 K_T \tag{21}$$

$$Q(n,V) = \rho n^2 D^5 K_Q \tag{22}$$

$$Q_B(n,V) = \rho n^2 D^5 \eta_R K_Q \tag{23}$$

where T is the thrust of the propeller, Q is the torque of the propeller in open water, and Q_B is the torque of the propeller considering ship's hull, n is the propeller speed, D is the diameter of the propeller, η_R is the propeller efficiency ($= 0.98$), K_T is the thrust coefficient, and K_Q is the torque coefficient. Coefficients, K_T and K_Q, should be defined from the experiment data for the ship. However, the detail of thrust and torque properties cannot be obtained here. These values are modified from the B-series propeller models (Oosterveld, et al., 1975).

$$\begin{aligned} K_T &= \sum_{i=1}^{39} C_{Ti} J^{s_i} \left(\frac{P}{D}\right)^{t_i} \left(\frac{A_E}{A_O}\right)^{u_i} z^{v_i} \\ &= a_1 J^2 + b_1 J + c_1 \end{aligned} \tag{24}$$

$$K_Q = \sum_{i=1}^{47} C_{Qi} J^{s_i} \left(\frac{P}{D}\right)^{t_i} \left(\frac{A_E}{A_O}\right)^{u_i} z^{v_i} = a_2 J^2 + b_2 J + c_2 \quad (25)$$

where C_T, C_Q, s, t, u, and v are the coefficients obtained from model experiments of the B-series propeller, P is the pitch of the propeller, A_E/A_O is the ratio of propeller area, z is the number of blades of the propeller, and J is an advanced constant that is expressed as

$$J = \frac{(1-w)V}{nD} \quad (26)$$

where w is the wake fraction and V is the speed of the ship (m/s). Further, the coefficients a_1, b_1, c_1, d_1, a_2, b_2, c_2, and d_2 are obtained for each ship using the least squares method.

3.5. Evaluation of Speed Loss

The speed of the ship is determined using the relation between the propulsion forces and the resistance forces. The propulsion forces consist of the reduced thrust in waves, and the resistance forces are divided into the wave resistance in still water and the added resistance. In still water, ships must satisfy the following relationship between the thrust and the resistance:

$$(1-t)T(V) = R_{SW}(V) \quad (27)$$

where t is the thrust reduction factor due to mechanical loss. The relation is expressed as

$$\beta_{TV}(n,h)(1-t)T(V) = R_{SW}(V) + R_{AW}(\omega,\chi,V) + R^A_{AW}(\omega,\chi,V) + R_{WD}(U_W,\theta_W) \quad (28)$$

When a ship sails in rough waves, the engine is usually controlled to prevent overload conditions. There are different types of engine controls, such as a constant speed control, constant revolution control, constant torque control, and constant power control. Constant speed control and constant revolution control do not seem to be realistic in rough waves; hence, they are not considered in this study. The other engine controls are modeled as follows (Hagiwara, et al., 2013):

$$Q_B(n,V) - Q_E(n_E) = 0 \quad (29)$$

$$R_{SW}(V) + R_{AW}(\omega,\chi,V) + R^A_{AW}(\omega,\chi,V) + R_{WD}(U_W,\theta_W) - \beta_{TV}(n,h)(1-t)T(V) = 0 \quad (30)$$

$$2\pi n Q_B(n,V) - P_E(n_E) = 0 \tag{31}$$

$$R_{SW}(V) + R_{AW}(\omega,\chi,V) + R^A_{AW}(\omega,\chi,V) + R_{WD}(U_W,\theta_W) - \beta_{TV}(n,h)(1-t)T(V) = 0 \tag{32}$$

where Q_E is the engine torque, n_E is the engine revolution, P_0 is the power of the ship in still water, and P_E is the power of the main engine. Simultaneous equations (29) and (30) for constant torque control, and equations (31) and (32) for constant power control, must be satisfied if these engine controls are used at sea. The engine torque satisfies the following relation with the propeller torque (Bondarenko, et al., 2010):

$$2\pi I_p \frac{dn}{dt} = Q_E(n_E,h_E) - Q_B(n,V) \tag{33}$$

$$Q_E(n_E,h_E) = Q_{MCR}(n_{MCR},h_{MCR}) \left\{ 0.5 \left(\frac{h_E}{h_{MCR}}\right)^{2/3} + 1.5 \left(\frac{h_E}{h_{MCR}}\right)^{1/3} \left(\frac{n_E}{n_{MCR}}\right) - \left(\frac{n_E}{n_{MCR}}\right)^2 \right\} \tag{34}$$

where I_p is the inertia moment of the rotating parts in the propeller shaft plus mass and added mass moment of inertia of the propeller and h_E is the fuel oil consumption of the main engine (g/kW/h). Further, Q_{MCR}, n_{MCR}, and h_{MCR} are the engine torque, engine revolution, and fuel oil consumption at the maximum continuous rating (MCR). No reduction gear is installed for the 28,000DWT bulk carrier here, and the relation $n \sim n_E$ is satisfied. In constant torque control, the engine revolution and fuel injection are determined to equalize $Q_B(n,V)$ and $Q_E(n_E,h_E)$. They are automatically controlled in the governor by monitoring the engine loads or combustion. It is important to consider the detailed information of the fuel notch in numerical simulations. However, no such records or data are available in the engine log book, etc. The engine torque, engine power, and fuel oil consumption are estimated from the characteristic curve provided by the manufacturer. The characteristic curve on the fuel oil consumption is only shown if the engine power is larger than 2,000 kW. Eqs. (35) and (36) are only valid at $P_E \geq$ 2,000 kW.

$$P_E(n_E) = 2\pi n_E Q_E(n_E,h_E) = p_1 n_E^3 \quad (\text{for } P_E \geq 2,000kW) \tag{35}$$

$$h_E = p_2 P_E(n_E)^3 + p_3 P_E(n_E)^2 + p_4 P_E(n_E) + p_5 \quad (\text{for } P_E \geq 2,000kW) \tag{36}$$

The relation $n \sim n_E$ can be applied for the bulk carrier. Eq. (35) gives the estimation of the engine power, while Eq. (36) gives the estimation of the fuel oil consumption. If these estimated values are substituted into Eq. (35), the value of P_E can be finally determined. The coefficients p_1, p_2, p_3, p_4, and p_5 are defined from measured data by using the least squares method. The wave states are irregular in an actual sea, and the speed loss under irregular sea states must be considered. The longitudinal motion (speed of the ship) can be expressed as follows (Prpić-Oršić, et al., 2012):

$$(M + m_{11}(\omega_i)) \frac{dV}{dt} = T_T(H_i, \omega_i, \chi, V) - R_T(H_i, \omega_i, \chi, V) \tag{37}$$

$$\begin{aligned} T_T(H_i, \omega_i, \chi, V) &= \beta_{TV}(1-t)T(n, V) && (38) \\ R_T(H_i, \omega_i, \chi, V) &= R_{SW}(V) + R_{AW}(\omega, \chi, V) + R^A_{AW}(\omega, \chi, V) \\ &+ R_{WD}(U_W, \theta_W) && (39) \end{aligned}$$

where M is the mass of the ship, $m_{11}(\omega)$ is the added mass in surge mode at the i-th angular frequency in the time series of the wave, T_T is the total thrust, and R_T is the total resistance. The damping force connected with surge oscillatory motion is relatively small in the longitudinal direction and is hence ignored in this study. In an irregular sea state, Eq. (37) must be solved in the time domain. As shown in Figure 4, wave series have different amplitudes and periods for each component. Based on Hsu's assumption (Hsu, et al., 1970), the added resistance (wave drift force) in irregular waves can be approximated as a series of regular waves with different amplitudes and periods. Each regular wave is a combination of two neighboring waves of half wave length. The zero-up cross method is used to analyze the wave series. Eq. (37) is numerically solved using the fourth order Runge-Kutta method. Eqs. (29) $\sim$ (32) are considered in each step of the integration. Time series of irregular waves are regarded as the combination of different regular wave components. The added resistance is computed in the i-th different wave period, T_i, and height, H_i. The time step of numerical integration is defined as T_i, which varies in each wave of 2-16 s. Once the speed of the ship, V, is obtained, the thrust, torque, engine power, and fuel consumption can be determined simultaneously. To solve Eq. (37) with engine controls, numerical procedures are considered as follows. In constant torque control, Eq. (26) is transformed into a function of n, V, and h_E by substituting Eqs. (23), (25), and (34).

$$0.1\rho D^3 \left\{ a_2(1-w)^2 V^2 + D b_2 (1-w) V n + D^2 c_2 n^2 \right\} - Q_E(n_E, h_E) = 0 \tag{40}$$

Eq. (40) can be regarded as the second-order algebraic equation with an unknown variable n when we compute the value of $T_T(H_i, \omega_i, \chi, V)$.

$$\alpha_1 n^2 + \alpha_2 n + \alpha_3 = 0 \tag{41}$$

where the coefficients α_1, α_2, and α_3 are expressed as

$$\begin{aligned} \alpha_1 &= 0.1\rho D^5 c_2 \\ \alpha_2 &= 0.1\rho D^4 b_2 (1-w) V \\ \alpha_3 &= 0.1\rho D^3 a_2 (1-w)^2 V^2 - Q_E(n_E, h_E) \end{aligned} \tag{42}$$

Eq. (41) is solved by the iterative Newton-Raphson method, and the value of n is determined. As the relation $n_E \sim n$ is satisfied, the values of h_E and P_E are fixed by Eqs. (35) and (36). If the procedure is iterated in each time step, the speed loss can be analyzed in constant torque control. In constant power control, Eq. (29) is transformed into the third-order algebraic equation with unknown variable n.

$$\alpha_4 n^3 + \alpha_5 n^2 + \alpha_6 n + \alpha_7 = 0 \tag{43}$$

where the coefficients α_4, α_5, α_6, and α_7 are expressed as

$$\begin{aligned} \alpha_4 &= 2\pi\rho D^5 c_2 \\ \alpha_5 &= 2\pi\rho D^4 b_2 (1-w) V \\ \alpha_6 &= 2\pi\rho D^3 a_2 (1-w)^2 V^2 \\ \alpha_7 &= -P_E(n_E, h_E) \end{aligned} \tag{44}$$

Eq. (43) is solved using the same method as that for Eq. (41), and the value of n is obtained. The values of n_E, h_E, and P_E are obtained in each time step, and the speed loss can be analyzed in constant power control. Thus, the speed loss in an irregular sea state can be obtained to maintain constant values of torque or engine power. The revolution, thrust and engine power are simultaneously obtained in the time series analysis in Eq. (37). In the constant power control, they can obtained in Eqs. (43)(44) with Eq. (37).

4. Computed Results for Speed Loss

4.1. Computed Results of Added Resistance

Here, the speed loss is simulated and validated for the 28,000DWT bulk carrier in rough waves of the Southern Hemisphere. The main dimensions

of the ship are listed in Table 1, and the draft condition is half loaded. The offset of the ship is approximated from a similar model of a bulk carrier, as shown in Figure 5. The computed added resistances in three wave directions (0°, 30°, and 60°) are shown in Figure 6, which are obtained by the EUT and the NSM. The wave directions of 0°, 90°, and 180° are defined as bow (head sea state), beam (beam sea state), and stern (following sea state), respectively. The common non-dimensioned peak values are $4 \sim 17$ when the wave length, λ, is close to the ship length, L. On the other hand, the values for short wave lengths ($L/\lambda > 2$) are different in the EUT and the NSM. The NSM evaluates it to be below 0.5, whereas the EUT computes it as $1 \sim 4$. This factor may influence the evaluation of speed loss due to waves in the high frequency region. The computed results of the added resistance are shown in Figure 7 using the asymptotic formulas of Faltinsen and Okusu (Faltinsen, et al., 1980) (Okusu, 1986) in the three wave directions. The formula of Faltinsen evaluates it as $2 \sim 4$, whereas the formula of Okusu evaluates it as $2 \sim 6$, where $2 < L/\lambda < 8$. If these computed results are added to those of the NSM, they become relatively similar to those of the EUT. The influence of a short wave length is not significant for a container ship (slender shape) (Faltinsen, et al., 1980); however, asymptotic analysis must be considered for a bulk carrier if the NSM is used. The difference in speed loss in this regard will be discussed later.

4.2. Computed Results of Thrust and Resistance in Still Water

In Eqs. (21) and (22), the coefficients of the second-order polynomials are obtained as $a_1 = -0.146, b_1 = -0.2576, c_1 = 0.2929$ and $a_2 = -0.0196, b_2 = -0.0184, c_2 = 0.0309$, respectively. Figure 8 shows the estimated results of the thrust and torque coefficients, K_T and $K_{QB} = \eta_R K_Q$, and the resistance and thrust in still water for the 28,000DWT bulk carrier. The values of K_T and K_{QB} are $0 \sim 0.3$ and $0 \sim 0.03$, respectively. The resistance in still water, $R_{SW}(V)$, varies from 0 to 500 kN below a navigation speed of $14 \sim 15$ knots. The reduced thrust also varies from 400 to 600 kN, which implies that these empirical models can reproduce the measured values for the bulk carrier.

4.3. Computed Results of of Wind and Wave

The authors have already summarized detailed results for winds and waves using numerical simulation models and a meteorological database for Cases A and B (Lu, et al., 2017). As mentioned previously, three different

wind conditions are compared (see Table 2). NCEP-FNL contains global meteorological information provided by NCEP, and it covers every 1° and 6 h. The ERA interim contains global meteorological information from ECMWF, and it covers every 0.7° and 6 h. First, wind distributions are constructed every 0.5° as global (outer region) and every 0.1° as inner region where the ship is located. The linear interpolated wind conditions are also compared with the wind condition of the inner region computed by the WRF (The Weather and Research Forecasting) physical air model (Shamarock, et al., 2008). The wave conditions are numerically simulated for three wind conditions using the global model Wave WATCH III (WW3) (Tolman, 2002). A two-way nesting technique is applied at the boundary between the inner and outer regions. The measured and simulated results of wind directions and speeds for the ship in Cases A and B are shown in Figures 9 and 10. The simulated waves are compared with the waves measured by radar on the ship for Cases A and B, as shown in Figures 11 and 12. In Case A, there are differences of 1 $\sim$ 3 m in the wave height and -30 $\sim$ -60° from the ship's bow in the wave direction. The corresponding differences in Case B are 1 m and 0 $\sim$ 60°. The simulated results are obtained as a directional spectrum, and they can generate a time series of a wave as follows:

$$\eta(t) = \sum_{i=1}^{N} \sqrt{S(\omega_i)\Delta\omega}\cos(\omega_i t - \epsilon_i) \tag{45}$$

$$S(\omega) = \int_0^{2\pi} D(\omega, \theta_{WV}) d\theta \tag{46}$$

where $S(\omega)$ is the frequency spectrum of the waves, $D(\omega, \theta)$ is the directional spectrum of the waves obtained by the WW3 model, θ_{WV} is the true wave direction, t is the time, ϵ is the phase angle with random generation, and N is the number of wave components. The time period of a wave series is set to 3 h to maintain the stationary state of the wave series. The wave conditions for numerical simulations of speed loss are summarized in Tables 3 and 4.

4.4. Speed Loss in Irregular Waves

The speed loss is numerically analyzed for the simulated waves, as summarized in Tables 3 and 4. As shown in the previous section, the thrust of the ship decreases if the submergence of the propeller is insufficient because of relative vertical motion. The estimated values of the reduced thrust factor, β_{TV}, are shown for Cases A and B in Figure 13. The average values of

β_{TV} are 0.82 $\sim$ 0.86 with the EUT and 0.89 $\sim$ 0.93 with the NSM in Case A, while they are 0.69 $\sim$ 0.75 with the EUT and 0.75 $\sim$ 0.78 with the NSM. Estimated values of β_{TV} is larger in Case B. The EUT tends to estimate the thrust reduction factor to be 0.1 less than that estimated by the NSM.

The simulated speeds of the ship for Cases A-1-2, A-2-2, A-3-2, A-1-4, A-2-4, A-3-4, A-1-6, A-2-6, and A-3-6 are computed in two wave directions (30° and 60°) in Figures 14-16. In Figure 14, the speed loss of 2 $\sim$ 3 knots is simulated in each hindcasted wave and wave direction. There are very small differences among the four simulation methods of added resistance. On the other hand, the simulated speeds are different in each wave condition in Figures 15 and 16, when the wave heights are 4 $\sim$ 7 m. The speed is zero in some parts of these figures. Hence, the total resistance is larger than the thrust. In actual ships, engine power might be additionally applied to generate forward speed. This factor cannot be considered in the simulation of engine control. In particular, the speed loss becomes larger if the asymptotic formulas of added resistance are additionally considered. The speed is higher by 1 $\sim$ 4 knots in these cases, when the wave direction varies from 30° to 60°. The ship heading varies in this range of directions, and the measured value should exist between these wave directions. The significant wave height differs by 1 $\sim$ 3 m here, and it also leads to a difference of 4 $\sim$ 6 knots in speed. The simulated speeds of the ship for Cases B-1-7, B-2-7, B-3-7, B-1-8, B-2-8, and B-3-7 are computed for two wave directions (30° and 60°) in Figures 17 and 18. The speed loss is overestimated in Cases B-1-7 and B-1-8, which is based on the estimated wave using NCEP data. The authors have already shown that NCEP overestimates the actual situation (Lu, et al., 2017), and the result is the same in the case of speed loss. The other results are relatively similar, and the speed increases by 1 $\sim$ 2 knots when the wave direction varies from 30° to 60°. There are very small differences among the simulation methods of added resistance in these cases. The simulated engine revolutions are also compared for Cases A-1-6, A-2-6, A-3-6, B-1-8, and B-2-8 in Figures 19 and 20. The simulated results are 95 $\sim$ 105 rpm, which are in good agreement with the measured values in Figures 1 and 2. The average values of the ship's speed, engine revolution, and engine power are calculated and compared with the measured results in Cases A and B, as shown in Figures 21-26. It is obvious that the speed losses are overestimated in Case A-1 (NCEP) and Case A-3 (WRF) on 2 $\sim$ 3 days if the wave direction is 30°. The simulated results are in agreement within a difference of 1 knot for Case A-3 (WRF) in the wave direction of 60°. On

the other hand, the speed losses are overestimated in all the cases under Case B, especially in Case B-1 (NCEP). The same tendency is observed, i.e., the ship's speed differs at wave directions of 30° and 60° in Cases B-1 and B-3. There are small differences in the ship's speeds in each model of added resistance. However, the simulated speeds differ significantly if the wave direction is 30°, i.e., in a head sea state. The speed loss becomes larger when asymptotic models are additionally considered with the NSM. The estimated values are closer if the wave direction is 60° rather than 30° in Figures 21 and 22. The same tendency can be seen in the average revolutions. In Figure 23, the simulated revolutions are larger for 5 rpm in Case A. On the other hand, they are slightly smaller by $1 \sim 2$ rpm in Case B, as shown in Figure 24. The engine power is underestimated if the wave direction is 30° in Case A, and it agrees within 100 kW when the direction is 60°. It is not necessarily in agreement in the entire period in Case B, because the ship increases the engine power at $1 \sim 1.5$ days, as shown in Figure 26. These results indicate that the differences in weather simulations and wave direction have a greater influence on the speed loss than those of seakeeping models.

4.5. Estimation of Fuel Consumption and CO_2 Emission

The accuracy of estimation is validated for two rough sea voyages here, and the magnitude of error can be shown. The fuel oil consumption is one of the most important factors in the optimal ship routing, and is compared in each case. As shown in Eq. (36), the fuel consumption can be estimated from the third-order polynomial provided by its manufacturer. The gauge of fuel oil tank is also monitored in the measurement, and total consumption of fuel oil is available as the difference of gauge values. However, it contains components of fuel consumed by other auxiliary machines or generators, besides the main engine. The consumed volume of fuel oil, h_{EV}, is obtained as

$$h_{EV} = \frac{h_E P_E(n_E)}{\rho_{oil} \times 1000} \tag{47}$$

where ρ_{oil} is the density of fuel oil, which is defined here as 0.952 kg/ℓ. The coefficients in Eqs. (35) and (36) are obtained as $p_1 = 0.281 \times 10^{-2}, p_2 = 0.1 \times 10^{-9}, p_3 = -0.9 \times 10^{-6}, p_4 = -0.6 \times 10^{-3}$, and $p_4 = 183.68$. The consumed volume of fuel oil in Eq. (47) is compared with the volume in the fuel oil tank for Cases A and B, as shown in Figure 27. It is obvious that the measured values are equally larger than those in Eq. (47). The calculated root mean square values are 85.36 and 83.24 ℓ/h, respectively. It seems

reasonable to assume that fuel oil of 80 $\sim$ 85 ℓ/h is consumed in auxiliary machines, generators, etc. The consumed volume in Eq. (47) should be used for comparison with the estimated results in Cases A and B. The estimated results of fuel oil consumption are compared for two wave directions (30° and 60°) in Cases A and B, as shown in Figures 28 -29. There are small differences in the fuel oil consumption in each simulation method of added resistance in Cases A and B. However, in Case B, the simulated values are 70 $\sim$ 80 ℓ smaller (1.5 $\sim$ 2 days) than the actual ones. The ship increases the engine power during this period, and the engine power is set to a constant value in the numerical simulation. This factor might influence the underestimation, as shown in Figure 29. The CO_2 emission is also briefly estimated here and compared among the simulated results. A simple relation between the gas emission and the fuel oil consumption is proposed as follows.

$$CO_2 = \rho_{oil} h_{EV} \times GEF \tag{48}$$

where GEF is the gas emission factor based on mass (3.173 kg of CO_2 emission per kg of fuel oil). The fuel oil consumption and CO_2 emission are totally evaluated during the period in each simulation case, i.e., 45 h in Case A and 33 h in Case B. The total fuel oil consumption and CO_2 emission during the period are calculated as

$$h_{ET} = \sum_{i=1}^{N} h_{EVi} \Delta t_i \tag{49}$$

$$CO_{2T} = \sum_{i=1}^{N} CO_{2i} \Delta t_i \tag{50}$$

where h_{ET} is the total fuel oil consumption during the simulation period, CO_{2T} is the total CO_2 emission during the simulation period, Δt_i is the time interval between the i-th and $(i+1)$-th simulation points, and N is the number of simulated points ($N = 9$). As shown in the previous section, the ship's speed decreases significantly and the sailing distance varies in each weather condition. These parameters should be evaluated as values per nautical mile. The sailing distance during the period is obtained as

$$D_T = \sum_{i=1}^{N} V_i \Delta t_i \tag{51}$$

The fuel oil consumption and CO_2 emission per nautical mile are expressed as follows:

$$h_{EM} = \frac{h_{ET}}{D_T} \tag{52}$$

$$CO_{2M} = \frac{CO_{2T}}{D_T} \tag{53}$$

The computed results of these parameters, h_{EM} and CO_{2M}, are compared with the measured results in Cases A and B with two wave directions of 30° and 60°, as shown in Figures 30-33. In Cases A, the fuel oil consumption differs by $10 \sim 40$ ℓ per nautical mile in the wave direction of 30°. The differences in the ship's speed contribute to this result. On the other hand, there are small differences if the wave height is 60°. In Case B, the difference in fuel oil consumption is $10 \sim 20$ ℓ per nautical mile, which is less than that in Case A. The same result is obtained, i.e., the differences are small in each wave condition and numerical model of added resistance, if the wave direction is 60°. These patterns of differences are common in the evaluated values of CO_2 emission per nautical mile, as shown in Figures 32 and 33. The range of variation is $20 \sim 100$ kg per nautical mile in Case A and $20 \sim 50$ kg per nautical mile in Case B. However, the difference is less than 30 kg per nautical mile when the wave direction is 60°. The wave direction is simulated as $30 \sim 60°$, which varies in both cases. It has already been shown that the heading of the ship tends to vary more frequently in rough seas than in calm seas (Lu, et al., 2017). The speed loss should be evaluated by combining the simulated results in multiple wave directions, such as $30 \sim 60°$ here.

5. Conclusions

This study focused on changes in a ship's performance in rough sea voyages, and comparisons were made against measured results for a 28,000DWT bulk carrier in the Southern Hemisphere. The accuracy was validated for each practical simulation model of added resistance. The main conclusions can be summarized as follows.

(1) Three remarkable speed losses were measured in the Southern Hemisphere, and two of them seemed to be similar situations of the main engine. The power of the main engine showed a relatively constant value, although the ship's speed and engine revolutions were reduced significantly. These rough sea voyages were analyzed by approximation as constant power control of main engine.

(2) Although there are various estimation methods of the added resistance, four patterns were compared with each other. It is known that added resistance exists at $L/\lambda > 2.0$ because of the blunt shape of the ship. The NSM underestimates it, and it is reasonable to add the diffraction component of asymptotic formulas. The EUT can compute it accurately, and is not necessary to consider asymptotic formulas additionally.
(3) Thrust reduction factors were computed for simulated results of waves in rough sea navigations. They were found to vary with the wave condition, wave direction, and ship's speed, and the values were $0.6 \sim 1.0$. The average values of the EUT were $0.05 \sim 0.1$ smaller than those of the NSM. The total thrust was smaller when the relative vertical motion was evaluated by the EUT under rough sea conditions.
(4) The ship's speed in irregular waves was compared for each added resistance method, wave direction, and simulated wave in two rough sea voyages. There were small differences among the simulation methods if the significant wave height was less than $2 \sim 2.5$ m. On the other hand, the simulated ship's speeds were significantly different for each method, especially at a wave direction of 30°. It became zero in Case A-3-6, because the simulation was carried out as constant power control. Ships are found to increase the engine power in this situation from measured data; deliberate speed loss under human factors becomes necessary in extreme wave conditions. The estimated results of revolutions of the main engine have a similar tendency.
(5) The ship's average speeds were $5 \sim 6$ knots smaller in Cases A and B if the simulated wave conditions were overestimated by $2 \sim 3$ m at a wave direction of 30°. This result verifies the reasonability of wave estimation in the authors' previous study (Lu, et al., 2017). The difference was smaller when the wave direction was defined as 60° because the added resistance was smaller.
(6) The condition setting of the time series (spectrum) for the estimated waves and wave direction was found to influence the accuracy of speed loss rather than the difference in the simulation models for added resistance. In other words, considerable uncertainty remains in the estimation of rough waves in the Southern Hemisphere.
(7) The speed loss was numerically evaluated under the theory of constant power control for Cases A and B, and the simulated results of engine power decreased by $100 \sim 200$ kW as the wave condition became more severe. This might be attributed to the increased added resistance. The measured results showed that the ship generates extra engine power of $200 \sim 300$ kW in Cases

A and B. This factor cannot be considered in this study, and it is necessary to adopt an algorithm for the deliberate speed loss.
(8) The fuel oil consumption was compared in each case per nautical mile. They were 90 and 70 ℓ per nautical mile, estimated by Eq. (44), in Cases A and B, respectively. This implies that the magnitude of speed loss strongly influences the values of fuel oil consumption, e.g., there is a difference of 20 ℓ per nautical mile. Moreover, the uncertainty in weather estimation leads to an additional error of $10 \sim 20$ ℓ, especially at the head sea state of $0 \sim 30°$. There are small differences in each weather condition and simulation method at the oblique sea state of $30 \sim 60°$.
(9) The emission of CO_2 was estimated as $220 \sim 260$ kg per nautical mile in rough seas for $4 \sim 7$ m of significant wave height, especially in Cases A-3 (WRF) and B-1 (NCEP). It could vary by $50 \sim 100$ ℓ per nautical mile at a wave direction of 30°. Further, the differences were smaller (within 30 kg per nautical mile) at a wave direction of 60°. The speed loss should be evaluated by combining the simulated results in multiple wave directions from head sea to oblique sea states.

Acknowledgement

The authors wish to extend their gratitude to Shoei Kisen Kaisha, Ltd., for their cooperation in conducting onboard measurements of the 28,000DWT bulk carrier for six years. Further, we wish to express our appreciation for the ship crews and local agencies for their insightful advice during the onboard measurement. In addition, we would like to thank Dr. Renato Skejic, MARINTEK, Norway, for his guidance in evaluating marine engines. This study was conducted as "The International Collaboration on Strongly Nonlinear Fluid Structure Interactions and Nurturing Young Researchers in Ocean Engineering" ($2012 \sim 2014$, represented by Prof. Masashi Kashiwagi), Japan Society for the Promotion of Science (JSPS). This study was financially supported by Scientific Research (B) ($2012 \sim 2015$ and $2016 \sim 2018$, represented by Kenji Sasa) and Challenging Explanatory Research ($2015 \sim 2017$, represented by Kenji Sasa) under Grants-in-Aid for Scientific Research, JSPS. This study was also supported by the Croatian Science Foundation - project 8722 and the University of Rijeka (contract no. 13.09.1.1.05).

References

Bondarenko, O. and Kashiwagi, M., "Dynamic behavior of ship propulsion

plant in actual seas", *Journal of Japan Institute of Marine Engineering*, *Vol.45*, pp.1012-1016, 2010

Bondarenko, O. and Kashiwagi, M., "Statistical consideration of propeller load fluctuation at racing condition in irregular waves", *Journal of Marine Science and Techology*, *Vol.16*, pp.402-410, 2011

Butterworth, J., Atlar, M. and Shi, W., "Experimental analysis of an air cavity concept applied on a ship hull to improve the hull resistance", *J. Ocean Engineering*, *Vol.110*, *Part B*, pp.2-10, 2015

Dee, D. P., et al., "The ERA-interim reanalysis, configuration and performance of the data assimilation system", *Q. J. R. Meteorol. Soc.*, *Vol.137*, *No.656*, pp.553-597, 2011

Devanney, J., "The impact of the energy efficiency design index on very large VLCC design and CO2 emissions", *Ship and Offshore Structures*, *Vol.6*, *No.4*, pp.355-368, 2011

Faltinsen, O.M., "Sea loads on ships and offshore structures", *Cambridge University Press*, 328p., 1993

Faltinsen, O.M., Minsaas, K.J., Liapis, N. and Skjørdal, S., "Prediction of resistance and propulsion of a ship in a seaway", *Proceedings of the 13th Symposium on Naval Hydrodynamics*, pp.505-529, 1980

Fujino, M. and Sakurai, K., "On the evaluation of wave exciting roll moment by the strip method", *Journal of the Society of Naval Architects of Japan*, *Vol.152*, pp.125-137, 1982 (in Japanese)

Fujiwara, T., Ueno, M. and Nimura, T., "Estimation of wind forces and moments acting on ships", *Journal of the Society of Naval Architects of Japan*, *Vol.183*, pp.77-90, 1998 (in Japanese)

Hagiwara, S., Yamasaki, S., Yoshimura, Y. and Adachi, H., "Ship performance design", *Seizando Shoten*, 255p., 2013 (in Japanese)

Hanaoka, T., "Theoretical study on ship motions in head sea", *Collection of Papers of Dr. Tatsuro Hanaoka*, pp.53-107, 1976 (in Japanese)

Hanssen, G.L. and James, R.W., "Optimum ship routing", *The Journal of the Insititute of Navigation*, *Vol.13*, *No.3*, pp.253-272, 1960

Holtrop, J.A., "A statistical re-analysis of resistance and propulsion data", *Proceedings of the International Shipping Progress*, *Vol. 31*, pp.272-276, 1984

Holtrop, J.A. and Mennen, G.G.J., "An approximate power prediction method", *Proceedings of the International Shipping Progress*, *Vol. 29*, pp.166-170, 1982

Hsu, F.H. and Blenkarn, K.A., "Analysis of peak mooring force caused by slow vessel drift oscillation in random seas", *Proceedings of Ocean Technology Conference(OTC)*, *Vol.1*, pp.135-146, 1970

Kalnay, E., et al., "The NCEP/NCAR 40-year reanalysis project", *Bulletin of American Meteorology Society*, *Vol.77*, *No.3*, pp.437-471, 1996

Kashiwagi, M., "Calculation formulas for the wave-induced steady horizontal force and yaw moment on a ship with forward speed", *Reports of Research Institute for Applied Mechanics, Kyushu University*, *Vol.37*, *No.107*, pp.1-18, 1991

Kashiwagi, M., "Added resistance, wave-induced steady sway force and yaw moment on an advancing ship", *Ship Technology Research*, *Vol.39*, pp.3-16, 1992

Kashiwagi, M., Sugimoto, K., Ueda, T., Yamasaki, K., Arihama, K., Kimura, K. Yamashita, R., Ito, A. and Mizokami, S., "An analysis system for propulsive performance in waves", *Journal of Kansai Society of Naval Architect, Japan*, *No. 241*, pp.1-16, 2004 (in Japanese)

Kosmas, O.T. and Vlachos, D.S., "Simulated annealing for optimal ship routing", *Computers and Operations Research*, *Vol.39*, pp.576-581, 2012

Lin, Y.H., Fang, M.C. and Yeung, R.W., "The optimization of ship weather-routing algorithm based on the composite influence of multi-dynamic elements", *J. Applied Ocean Research*, *Vol.43*, pp.184-194, 2013

Lu, L.F., Sasa, K., Sasaki, W., Terada, D., Kano, T. and Mizojiri, T., "Rough wave simulation and validation using onboard ship motion data in the Southern Hemisphere to enhance ship weather routing", *J. Ocean Engineering* (Under Review)

Maki, A., Akimoto, Y., Nagata, Y., Kobayashi, S., Kobayashi, E., Shiotani, S., Ohsawa, T. and Umeda, N., "A new weather-routing system that accounts for ship stability based on a real-coded genetic algorithm", *Journal of Marine Science and Technology*, *Vol.16*, pp.311-322, 2011

Newman, J.N., "The theory of ship motions", *J. Advances in Applied Mechanics*, *Vol.18*, pp.221-283.

NYK (Nippon Yusen Kaisha), "NYK super eco ship 2030", *http://www.nyk.com/english/csr/envi/ecoship/*, 2009

Okusu, M., "Added resistance of blunt bow ships in very short waves", *Journal of Kansai Society of Naval Architect, Japan*, *No. 202*, pp.39-42, 1986

Oosterveld, M.W.C. and Van Oossanen, P., "Further computer-analyzed data of the Wageningen B-screw series", *Proceedings of International Shipping Progress*, *Vol.22*, *No.251*, pp.3-14, 1975

Prpić-Oršić, J. and Faltinsen, O.M., "Estimation of speed loss and associated CO2 emissions in a seaway", *J. Ocean Engineering*, *Vol. 44*, pp.1-10, 2012

Salvesen, N., Tuck, E.O., Faltinsen, O.M., "Ship motions and sea loads", *Transaction of the Society of Naval Architects and Marine Engineers*, *No.6*, pp.1-30, 1970

Skamarock, W. C., Klemp, J. B., Dudhia, J., Gill, D. O., Barker, D. M., Duda, M. G., Huang, X.-Y., Wang, W. and Powers, J. G., "A description of the advanced research WRF version 3., *NCAR Technical Note NCAR/TN-475+STR*, 113p., 2008

Smogeli, O.N., "Control of marine propellers from normal to extreme conditions", *Ph.D Thesis of Dept. of Marine Engineering and Science, NTNU*, 242p., 2006

Tolman, H.L., "Validation of WAVEWATCH III version 1.15 for a global domain", *NOAA/NWS/NCEP/OMB Technical Note*, *Nr. 213*, 33p., 2002

Vettor, R. and Guedes Soares, C., "Rough weather avoidance effect on the wave climate experienced by oceangoing vessels", *J. Applied Ocean Research*, *Vol.59*, pp.605-615, 2016

Yasuda, E., Iwashita, H. and Kashiwagi, M., "Improvement of Rankine panel method for seakeeping prediction of a ship in low frequency region", *Proceedings of the 35th International Conference on Ocean, Offshore and Arctic Engineering*, pp.1-9, 2016

Figure 1

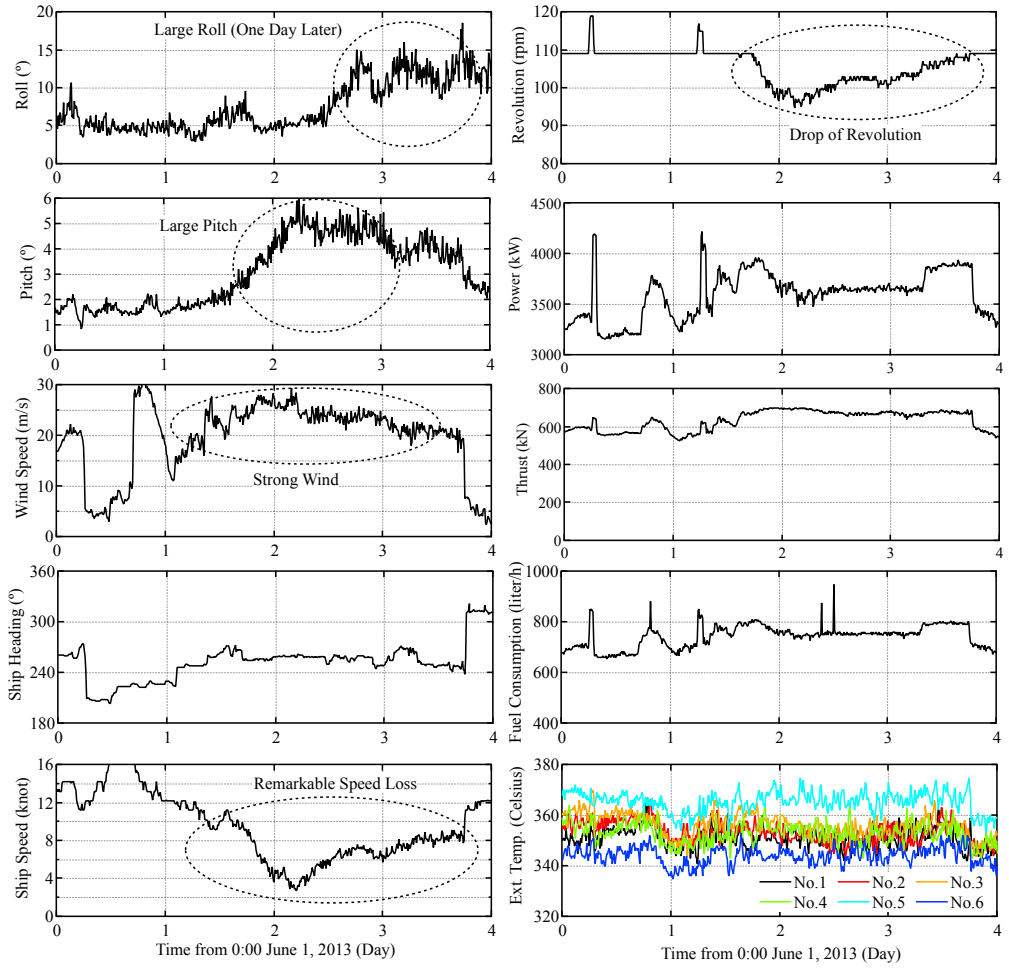

Figure 1: Variation of measured parameters in rough sea navigation in June 1-4, 2013 (Case A)

Figure 2

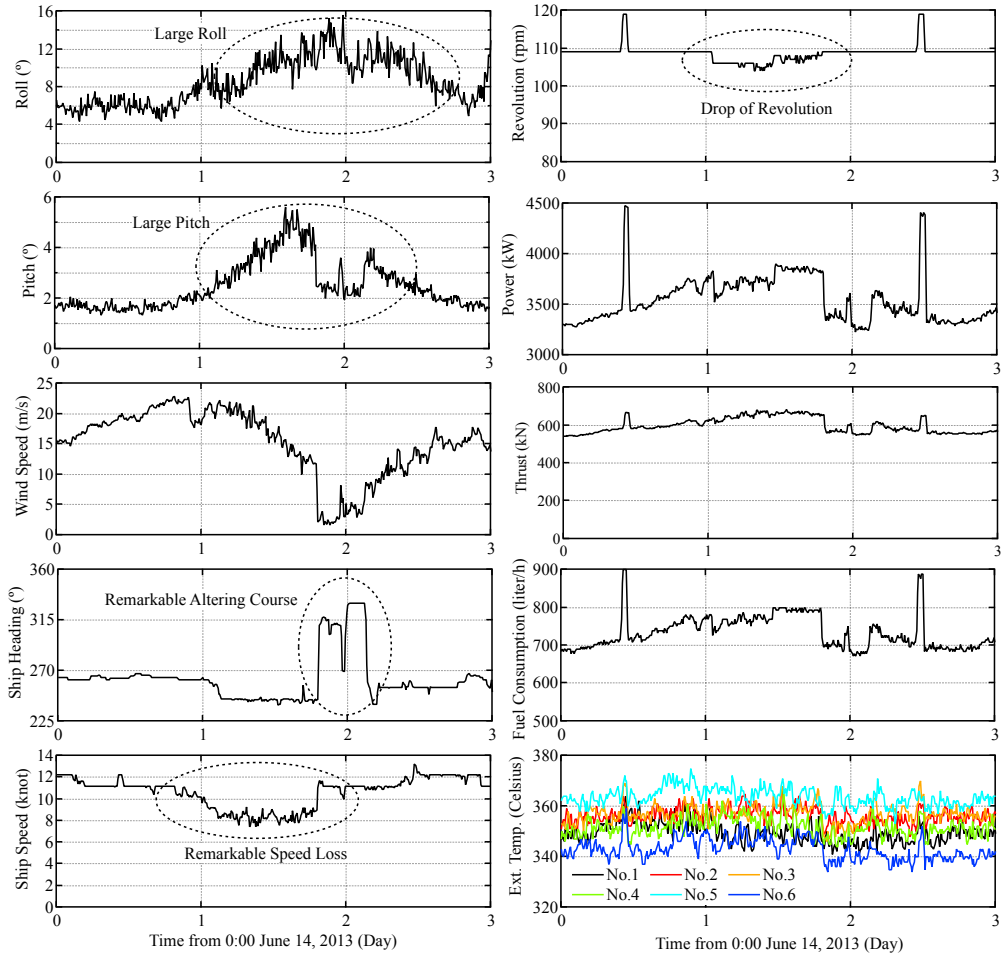

Figure 2: Variation of measured parameters in rough sea navigation in June 14-17, 2013 (Case B)

Figure 3

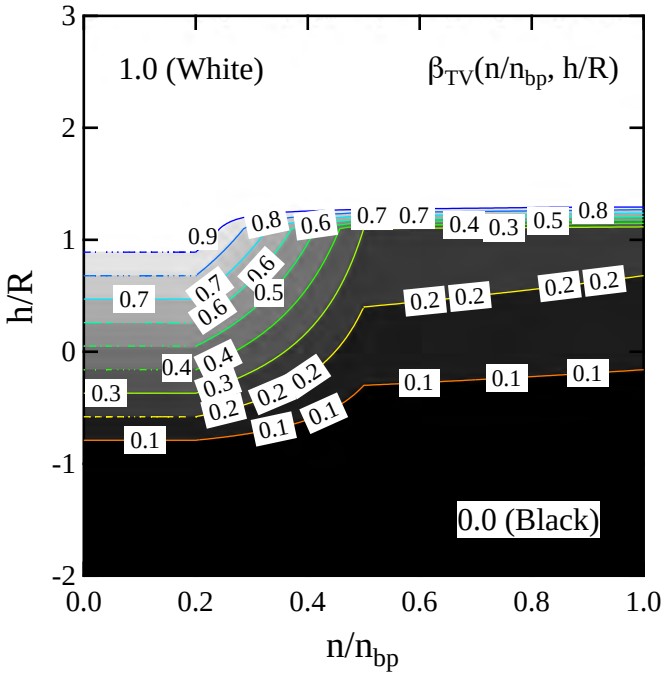

Figure 3: Approximated thrust deduction factor for open propeller (Smogeli)

Figure 4

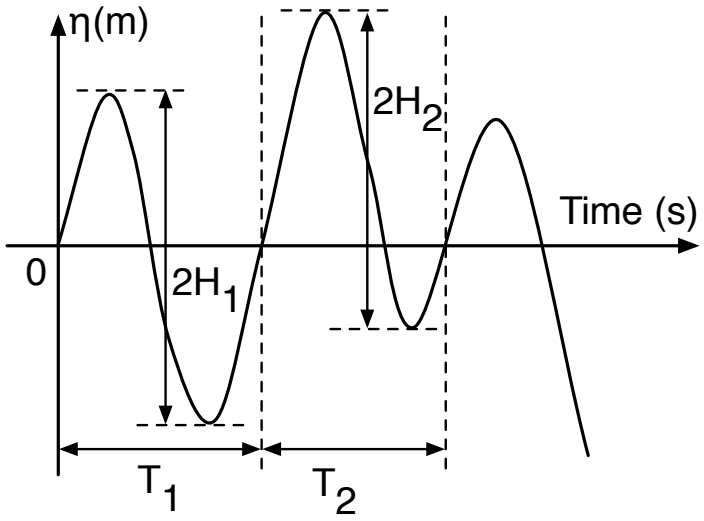

Figure 4: Approximation of wave drift force in irregular wave

Figure 5

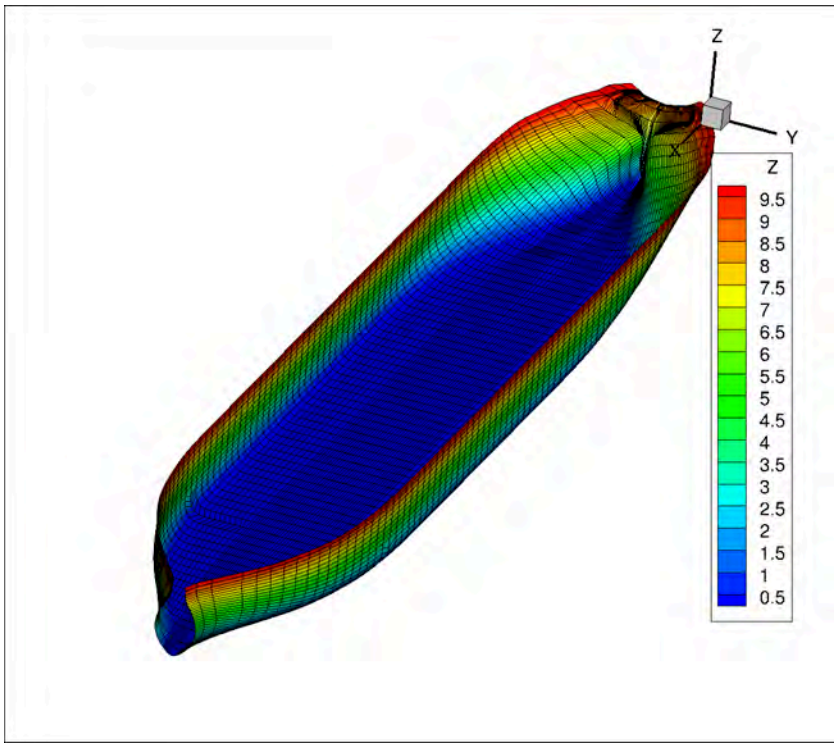

Figure 5: Approximated offset of 28,000DWT bulk carrier

Figure 6

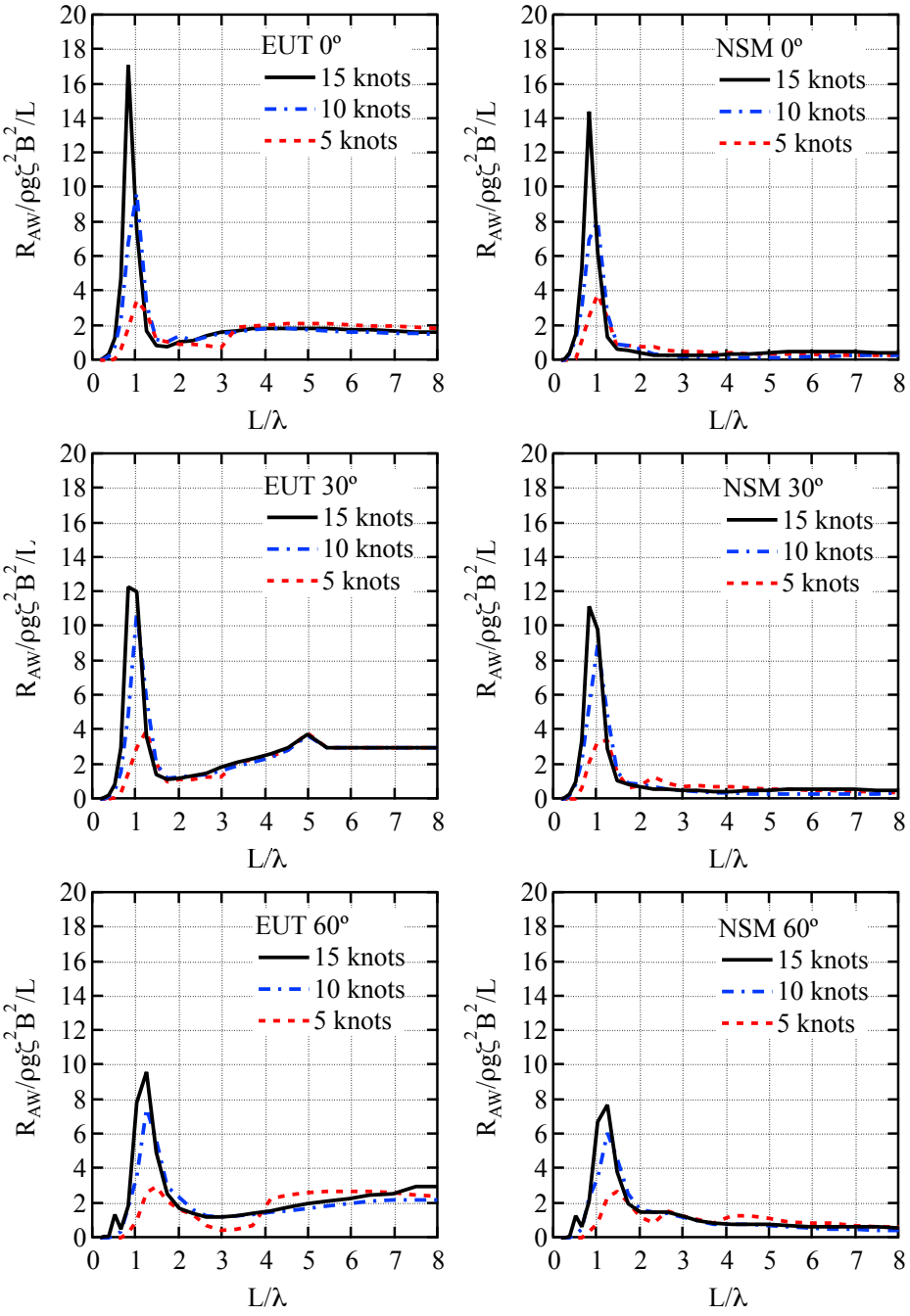

Figure 6: Comparison of added resistance for 28,000DWT bulk carrier (EUT and NSM, 0°, 30° and 60°)

Figure 7

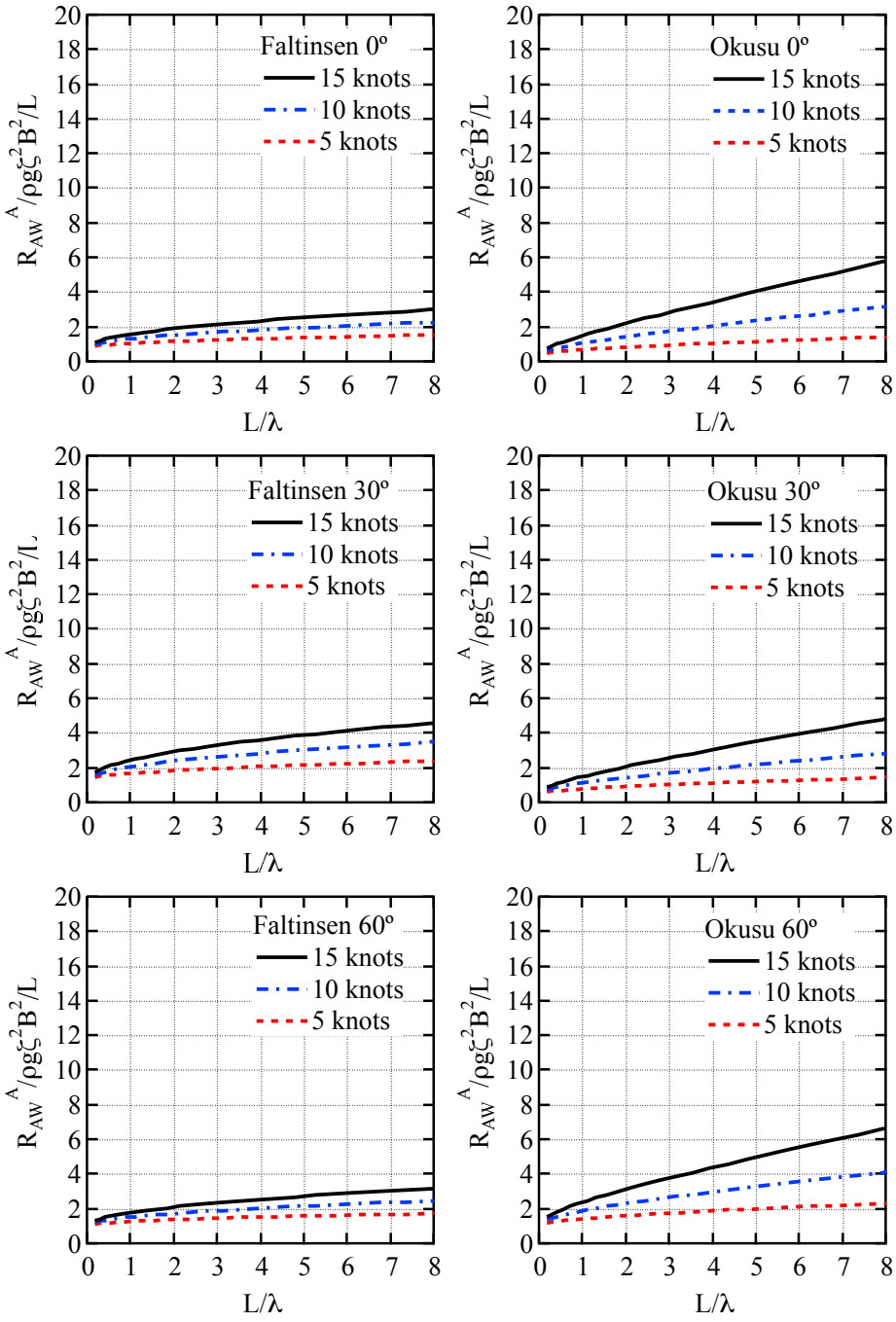

Figure 7: Comparison of added resistance for 28,000DWT bulk carrier (Asymptotic formulas, 0°, 30° and 60°)

Figure 8

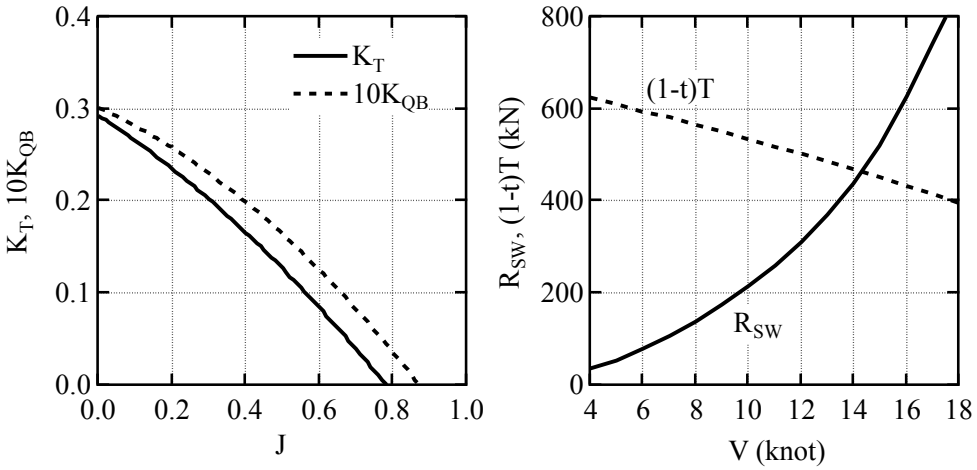

Figure 8: Estimated results of thrust and torque coefficients, resistance and thrust in still water

Figure 9

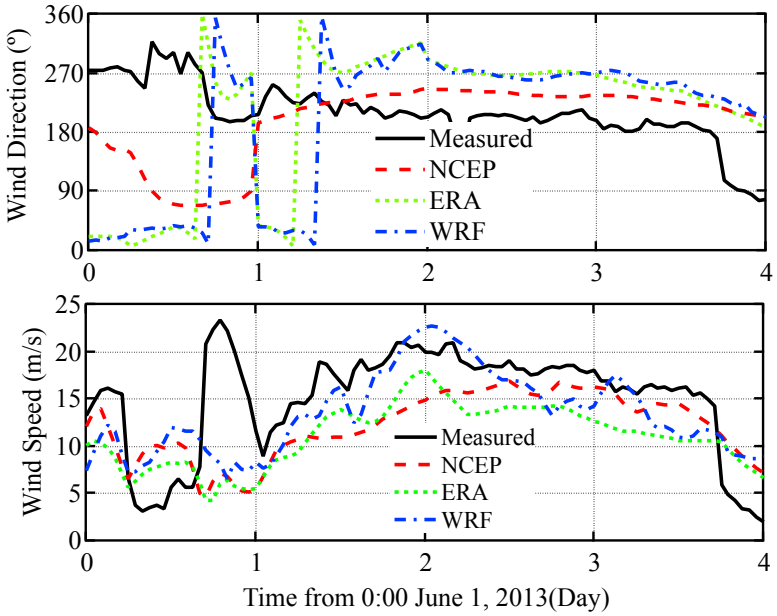

Figure 9: Comparison of simulated winds in Case A, June 1-4, 2013

Figure 10

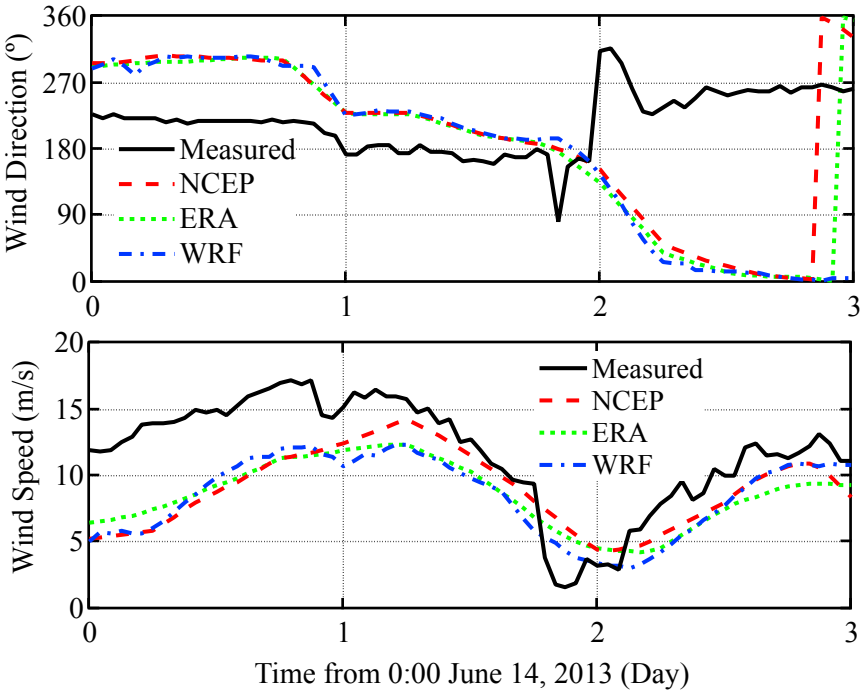

Figure 10: Comparison of simulated winds in Case B, June 14-16, 2013

Figure 11

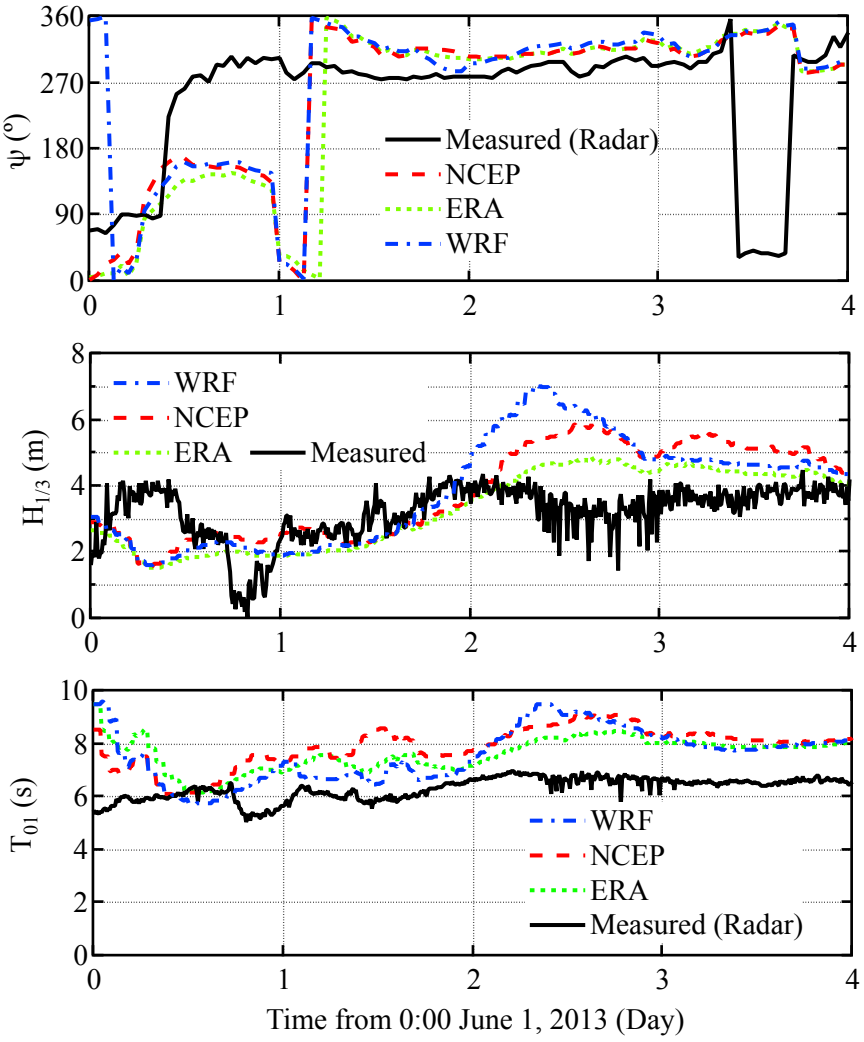

Figure 11: Comparison of simulated waves in Case A, June 1-4, 2013

Figure 12

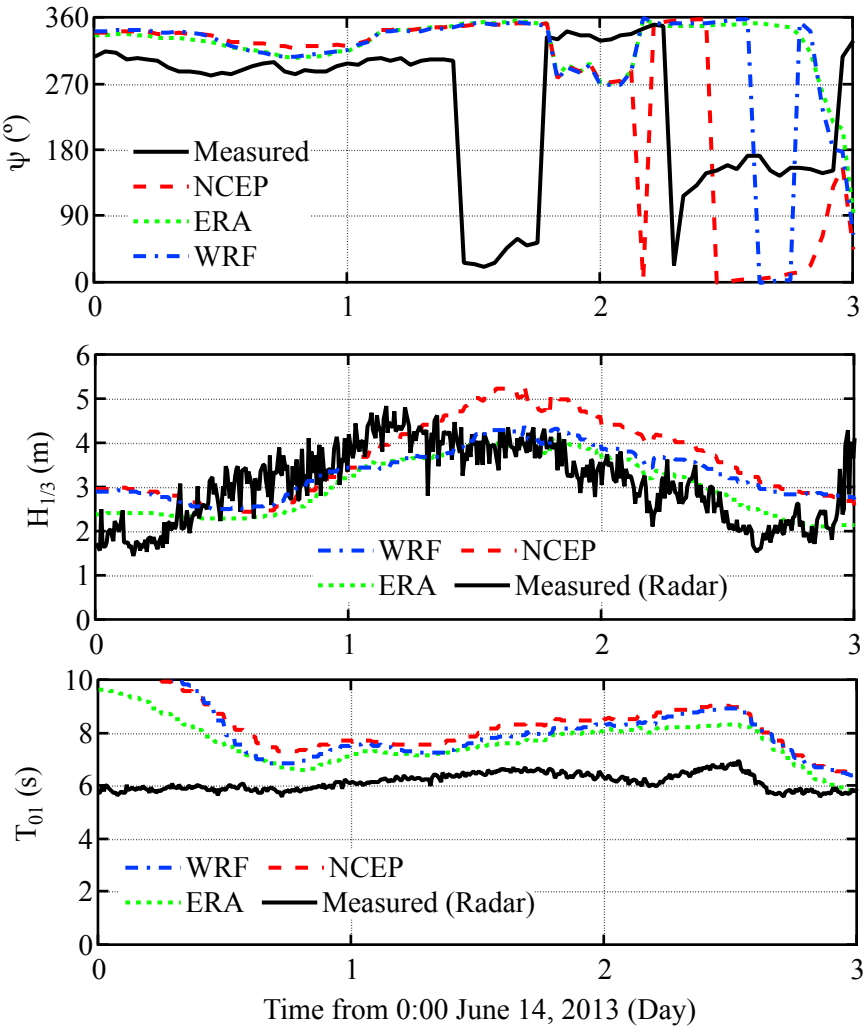

Figure 12: Comparison of simulated waves in Case B, June 14-16, 2013

Figure 13

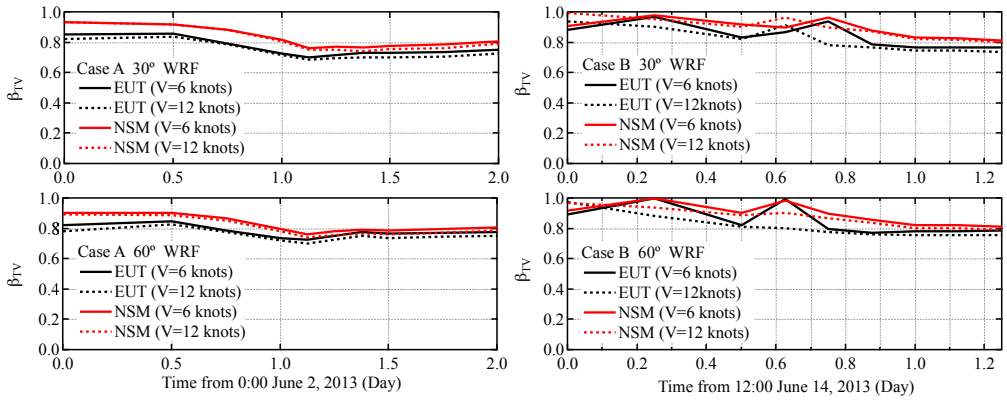

Figure 13: Estimated deduction factor of thrust using WRF (Cases A and B)

Figure 14

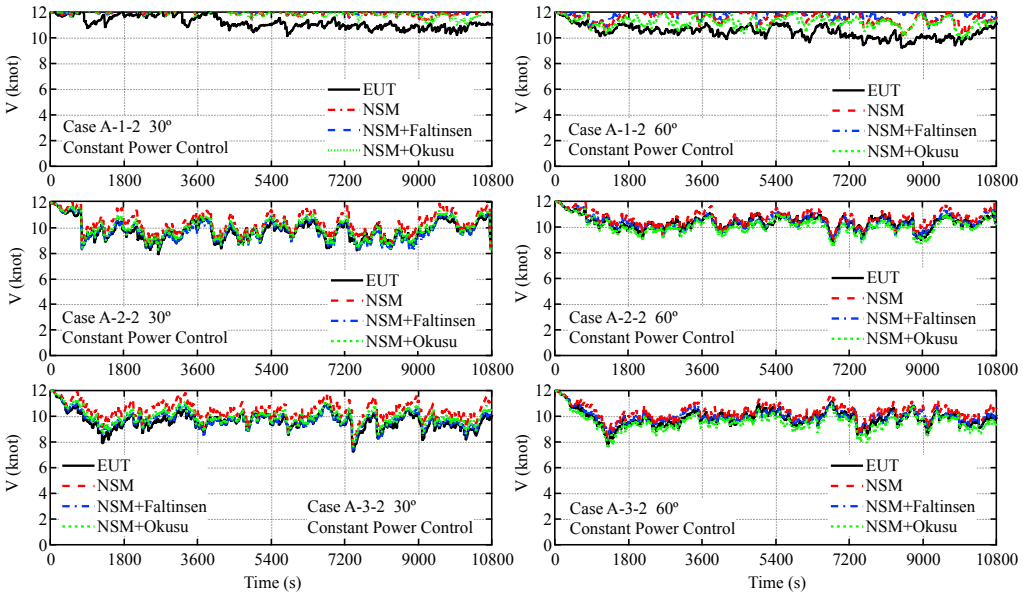

Figure 14: Estimated speed of ship in rough waves (Cases A-1-2, A-2-2, and A-3-2, 30° and 60°)

Figure 15

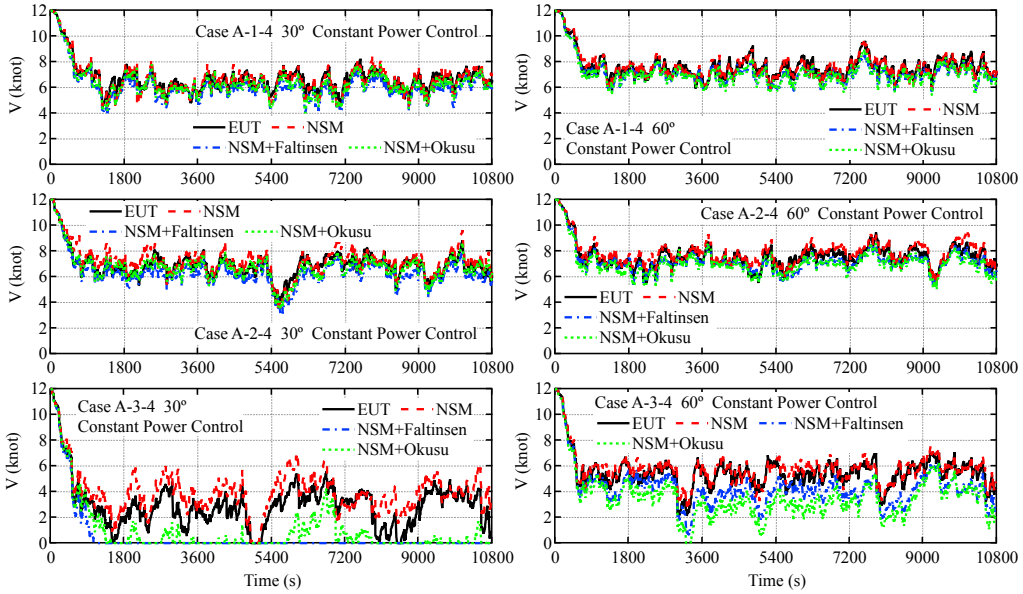

Figure 15: Estimated speed of ship in rough waves (Cases A-1-4, A-2-4, and A-3-4, 30° and 60°)

Figure 16

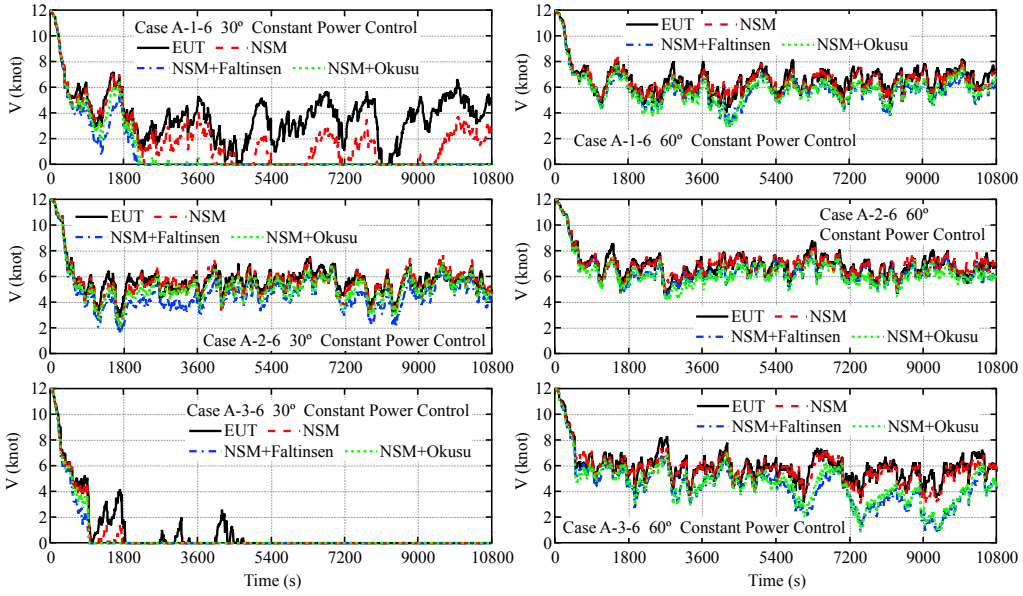

Figure 16: Estimated speed of ship in rough waves (Cases A-1-6, A-2-6, and A-3-6, 30° and 60°)

Figure 17

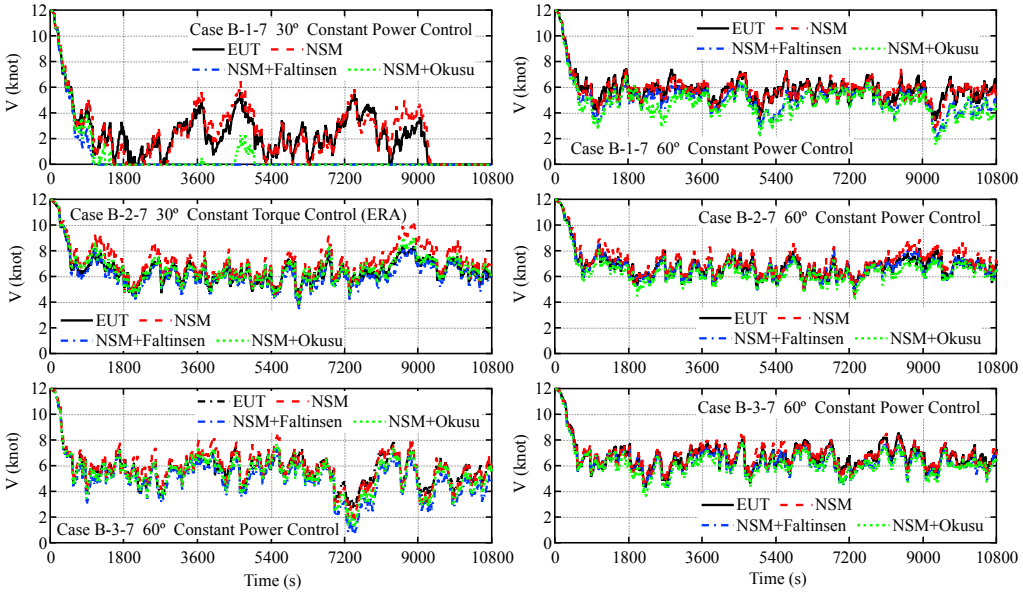

Figure 17: Estimated speed of ship in rough waves (Cases B-1-7, B-2-7, and B-3-7, 30° and 60°)

Figure 18

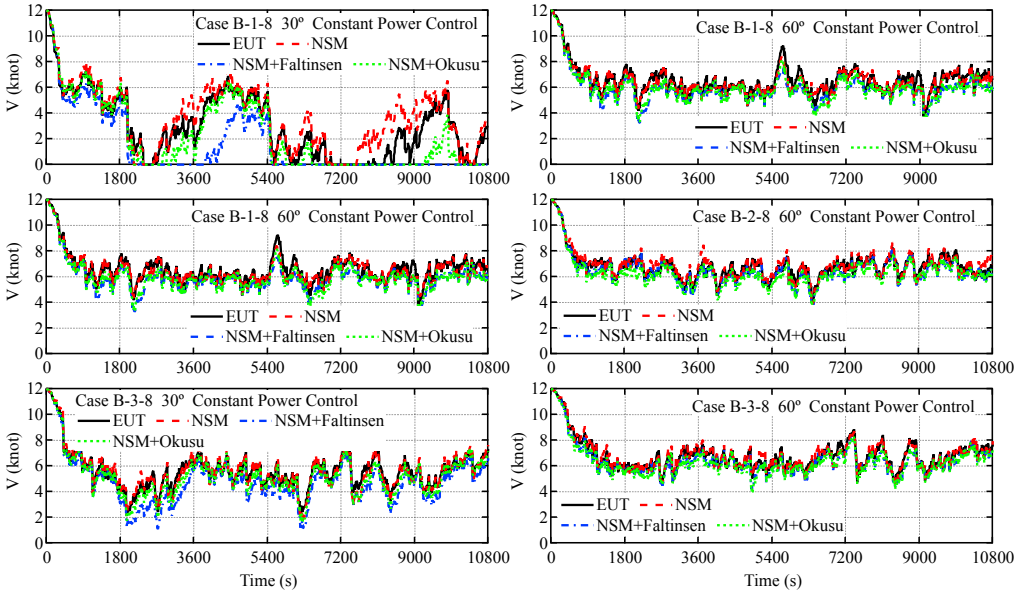

Figure 18: Estimated speed of ship in rough waves (Cases B-1-8, B-2-8, and B-3-8, 30° and 60°)

Figure 19

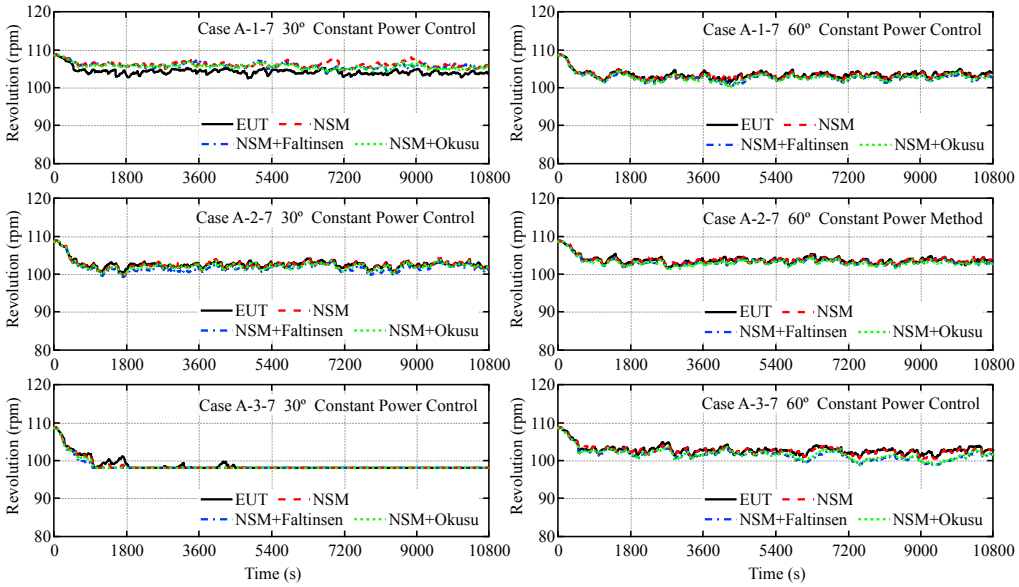

Figure 19: Estimated engine revolution in rough waves (Cases A-1-6, A-2-6, and A-3-6, 30° and 60°)

Figure 20

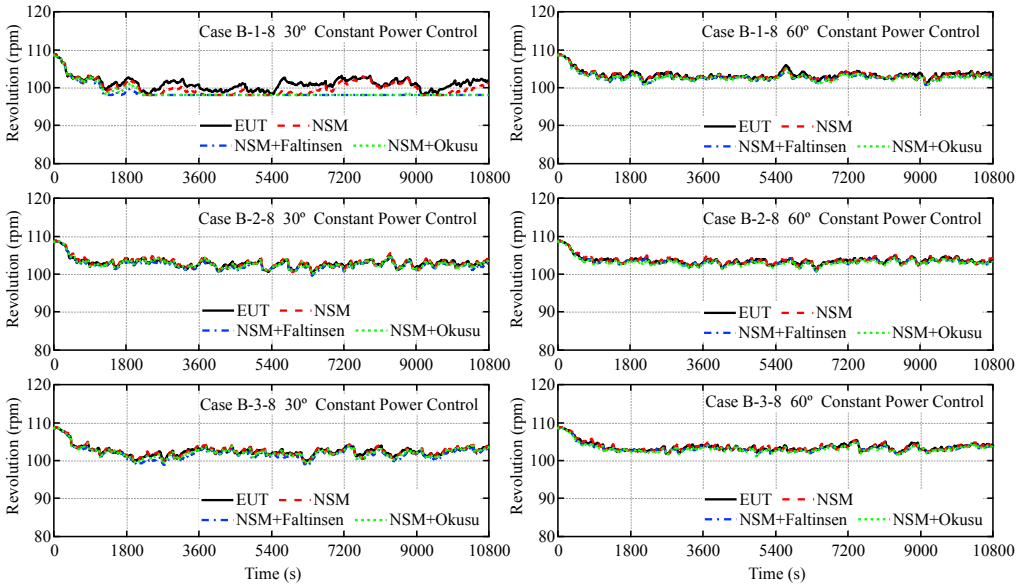

Figure 20: Estimated engine revolution in rough waves (Cases B-1-8, B-2-8, and B-3-8, 30° and 60°)

Figure 21

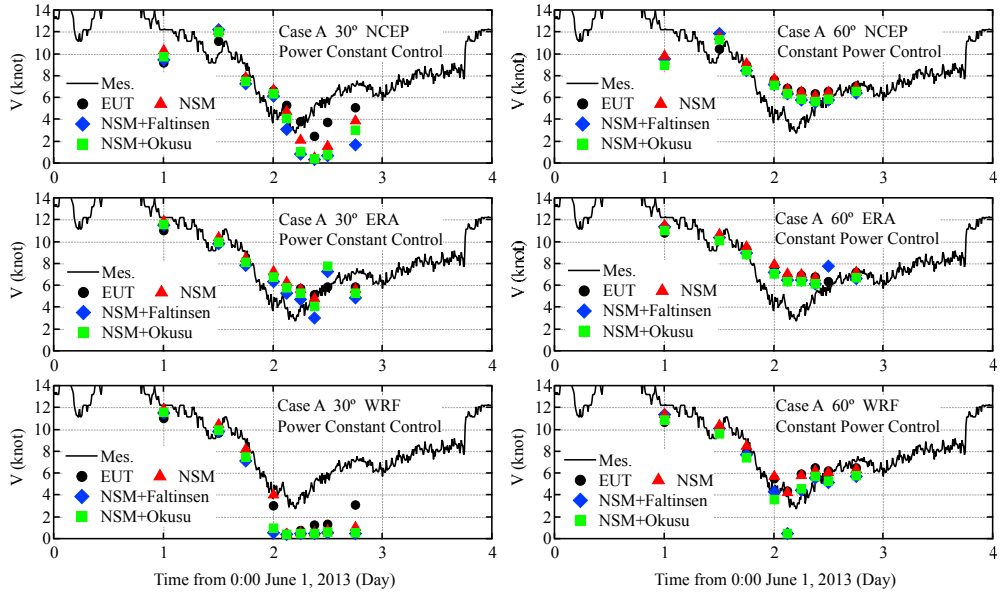

Figure 21: Comparison of averaged ship's speed between measurement and simulations in rough waves (Cases A, 30° and 60°)

Figure 22

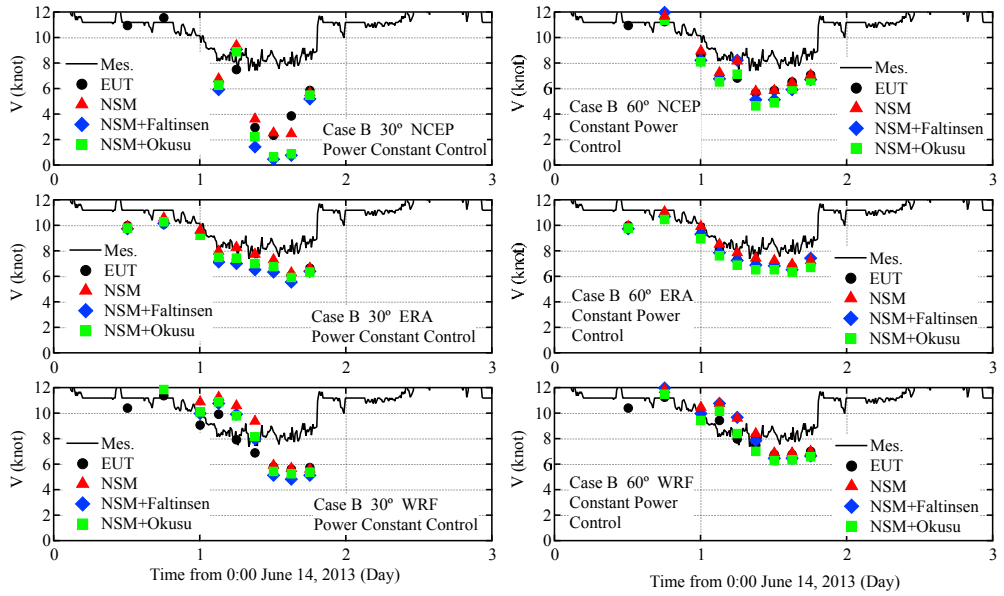

Figure 22: Comparison of averaged ship's speed between measurement and simulations in rough waves (Cases B, 30° and 60°)

Figure 23

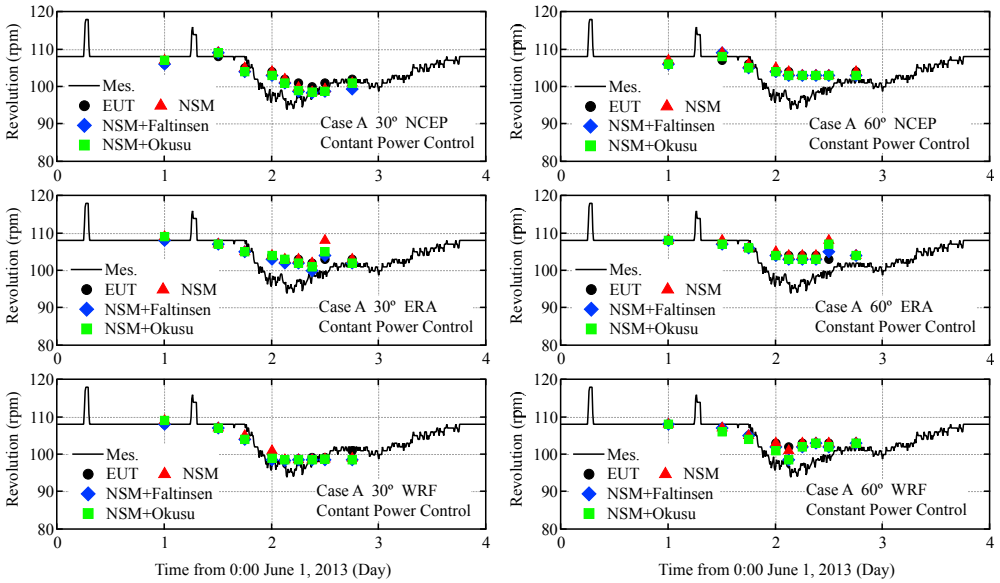

Figure 23: Comparison of averaged engine revolution between measurement and simulations in rough waves (Cases A, 30° and 60°)

Figure 24

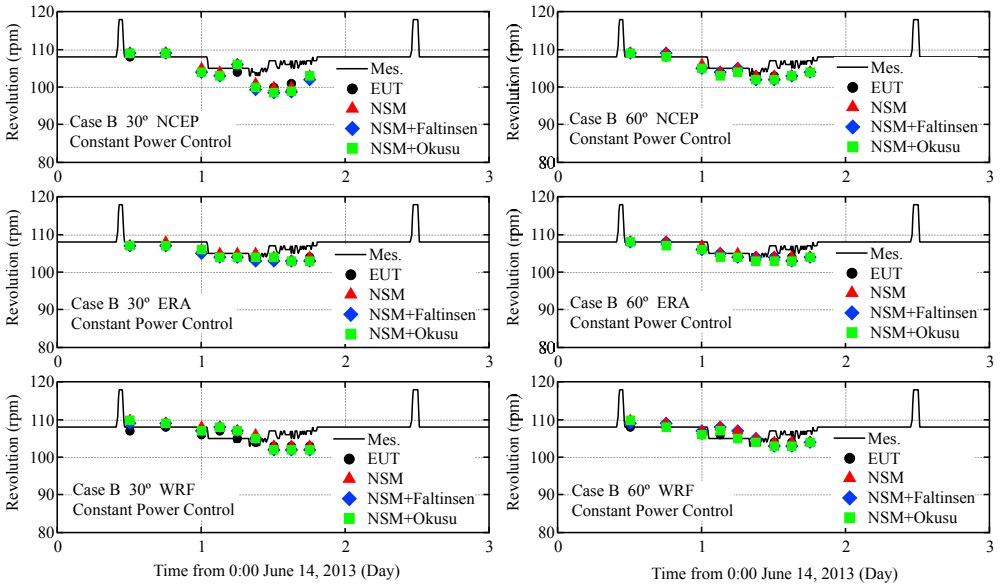

Figure 24: Comparison of averaged engine revolution between measurement and simulations in rough waves (Cases B, 30° and 60°)

Figure 25

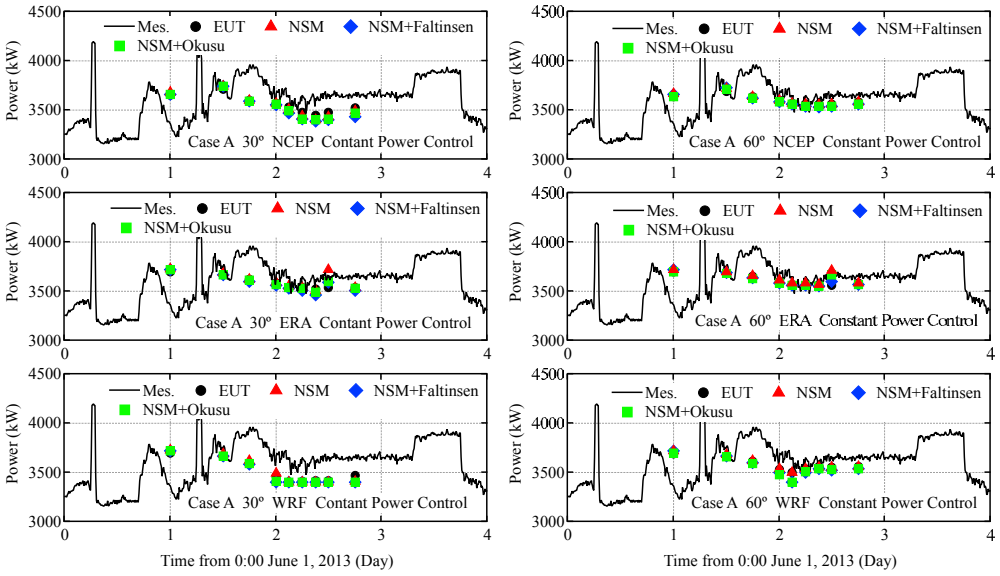

Figure 25: Comparison of averaged engine power between measurement and simulations in rough waves (Cases A, 30° and 60°)

Figure 26

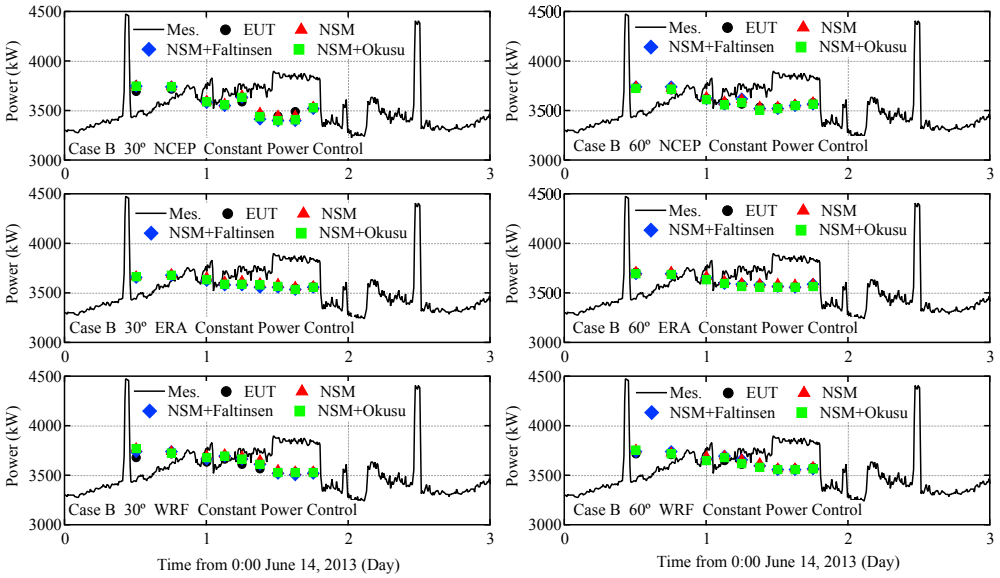

Figure 26: Comparison of averaged engine power between measurement and simulations in rough waves (Cases B, 30° and 60°)

Figure 27

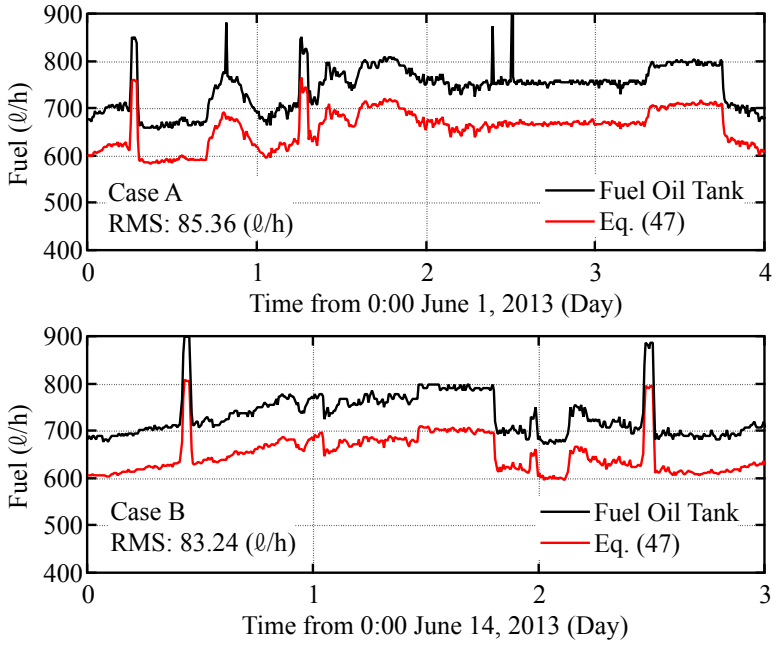

Figure 27: Comparison of consumed volume of fuel flow in Cases A and B)

Figure 28

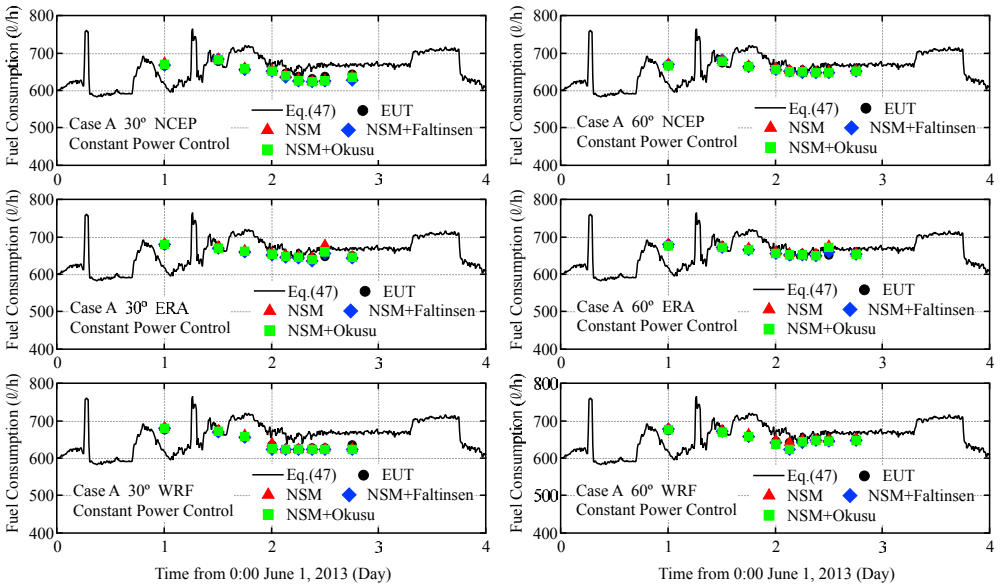

Figure 28: Comparison of fuel oil consumption between measurement and simulations in rough waves (Cases A, 30° and 60°)

Figure 29

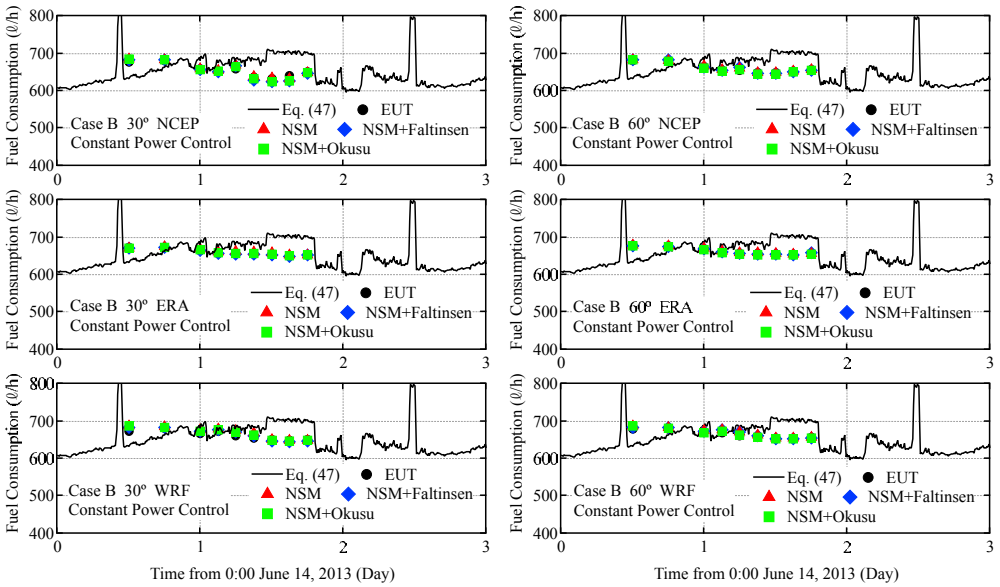

Figure 29: Comparison of fuel oil consumption between measurement and simulations in rough waves (Cases B, 30° and 60°)

Figure 30

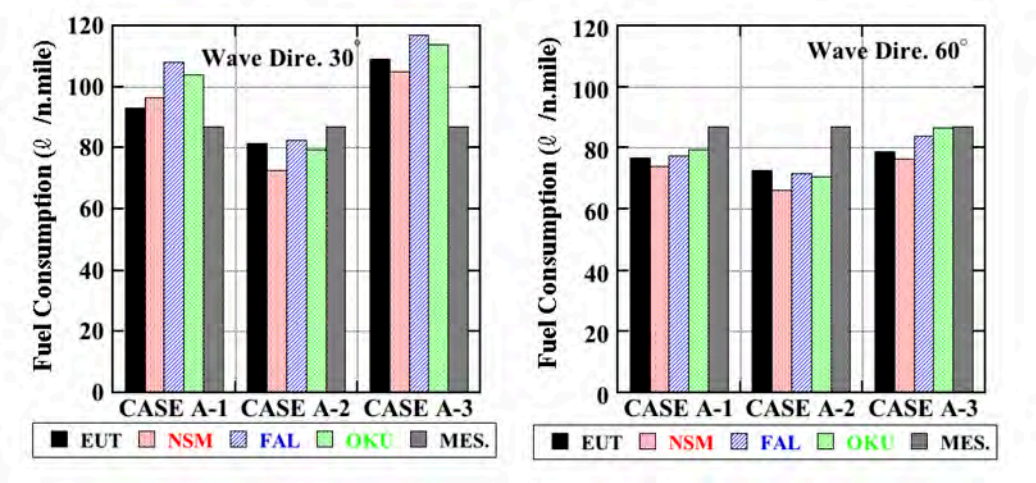

Figure 30: Comparison of fuel oil consumption per nautical mile between estimations and simulations in rough waves (Cases A, 30° and 60°)

Figure 31

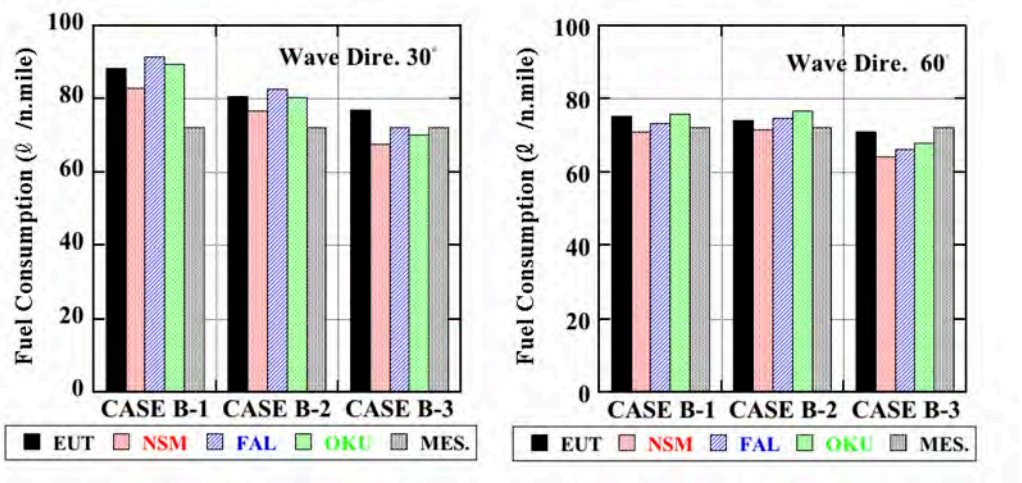

Figure 31: Comparison of fuel oil consumption per nautical mile between estimations and simulations in rough waves (Cases B, 30° and 60°)

Figure 32

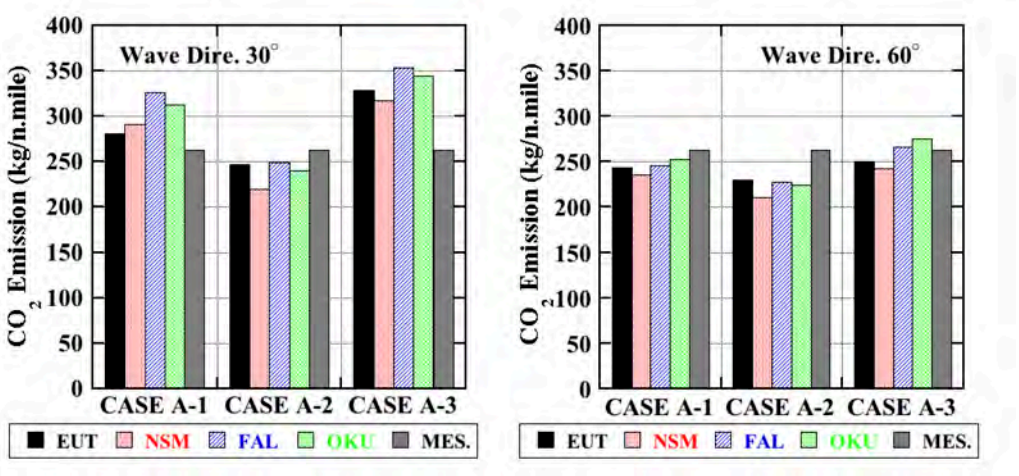

Figure 32: Comparison of CO_2 emission per nautical mile between estimations and simulations in rough waves (Cases A, 30° and 60°)

Figure 33

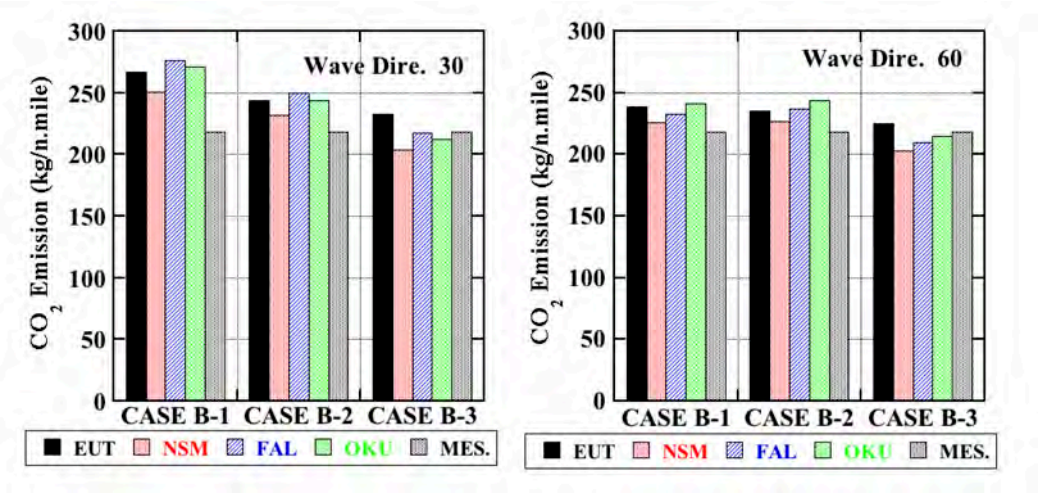

Figure 33: Comparison of CO_2 emission per nautical mile between estimations and simulations in rough waves (Cases B, 30° and 60°)

Table 1

Table 1: Main dimensions of 28,000DWT class bulk carrier

Length, between perpendiculars	160.4 m
Breadth	27.2 m
Draft (Case A and Case B)	8.16 m
Displacement (Case A and Case B)	28,280 t
Block Coefficient C_b	0.77
Prismatic Coefficient C_P	0.78
Operational Speed	12.0 knots
Main Engine	Diesel Engine with 6 cylinders
Maximum Continuous Rating (MCR)	5,850 kW $\times$ 129 rpm
Normal Rating (NOR)	4,970 kW $\times$ 122 rpm
Propeller	4 Bladed solid type (FPP)
Propeller Diameter	5.25 m
Propeller Pitch	3.864 m(0.7R) and 3.685 m (Mean)

Table 2

Table 2: Conditions of numerical simulations for winds and waves

Database	Wind simulation	Wave simulation
NCEP-FNL	Linear interpolation 0.5°(Global), 0.1°(Region)	WW3 0.5°(Global), 0.1°(Region)
ERA interim	Linear interpolation 0.5°(Global), 0.1°(Region)	WW3 0.5°(Global), 0.1°(Region)
NCEP-FNL	WRF 0.5°(Global), 0.1°(Region)	WW3 0.5°(Global), 0.1°(Region)

Table 3

Table 3: Wave conditions for numerical simulations of speed loss in Case A

Date and Time	NCEP	ERA	WRF
0:00 June 2, 2013	Case A-1-1 2.59 m, 7.37 s	Case A-2-1 1.89 m, 7.01 s	Case A-3-1 1.92 m, 7.32 s
12:00 June 2, 2013	Case A-1-2 2.41 m, 8.56 s	Case A-2-2 2.36 m, 7.25 s	Case A-3-2 2.45 m, 6.47 s
18:00 June 2, 2013	Case A-1-3 3.00 m, 7.55 s	Case A-2-3 2.86 m, 7.22 s	Case A-3-3 3.30 m, 6.71 s
0:00 June 3, 2013	Case A-1-4 3.73 m, 7.79 s	Case A-2-4 3.58 m, 7.23 s	Case A-3-4 4.96 m, 7.53 s
3:00 June 3, 2013	Case A-1-5 4.42 m, 8.12 s	Case A-2-5 3.91 m, 7.54 s	Case A-3-5 5.80 m, 8.19 s
6:00 June 3, 2013	Case A-1-6 5.27 m, 8.61 s	Case A-2-6 4.36 m, 8.00 s	Case A-3-6 6.56 m, 9.02 s
9:00 June 3, 2013	Case A-1-7 5.46 m, 8.69 s	Case A-2-7 4.63 m, 8.22 s	Case A-3-7 6.99 m, 9.49 s
12:00 June 3, 2013	Case A-1-8 5.62 m, 8.85 s	Case A-2-8 4.69 m, 8.23 s	Case A-3-8 6.34 m, 9.10 s
18:00 June 3, 2013	Case A-1-9 5.61 m, 9.10 s	Case A-2-9 4.80 m, 8.47 s	Case A-3-9 5.75 m, 8.78 s

Table 4

Table 4: Wave conditions for numerical simulations of speed loss in Case B

Date and Time	NCEP	ERA	WRF
12:00 June 14, 2013	Case B-1-1 2.66 m, 7.56 s	Case B-2-1 2.46 m, 6.83 s	Case B-3-1 2.68 m, 7.23 s
18:00 June 14, 2013	Case B-1-2 2.85 m, 6.85 s	Case B-2-2 2.57 m, 6.23 s	Case B-3-2 2.98 m, 6.64 s
0:00 June 15, 2013	Case B-1-3 3.64 m, 7.43 s	Case B-2-3 3.43 m, 6.97 s	Case B-3-3 3.58 m, 7.27 s
3:00 June 15, 2013	Case B-1-4 4.13 m, 7.47 s	Case B-2-4 3.69 m, 7.06 s	Case B-3-4 3.64 m, 7.17 s
6:00 June 15, 2013	Case B-1-5 4.46 m, 7.51 s	Case B-2-5 3.76 m, 6.97 s	Case B-3-5 3.86 m, 7.11 s
9:00 June 15, 2013	Case B-1-6 4.87 m, 7.73 s	Case B-2-6 3.86 m, 7.00 s	Case B-3-6 3.90 m, 7.12 s
12:00 June 15, 2013	Case B-1-7 5.51 m, 8.13 s	Case B-2-7 4.16 m, 7.25 s	Case B-3-7 4.49 m, 7.59 s
15:00 June 15, 2013	Case B-1-8 5.76 m, 8.42 s	Case B-2-8 4.28 m, 7.45 s	Case B-3-8 4.64 m, 7.76 s
18:00 June 15, 2013	Case B-1-9 5.32 m, 8.28 s	Case B-2-9 4.19 m, 7.59 s	Case B-3-9 4.40 m, 7.80 s